Pergamon

Prog. Aerospace Sci., Vol. 31, pp. 335–386, 1995

0376-0421/95/ $29.00

0376-0421(95) 00001-1

THE WELLS AIR TURBINE FOR WAVE ENERGY CONVERSION

S. Raghunathan

Department of Aeronautical Engineering, Queens's University, Belfast, BT71NN, U.K.

(Received 17 January 1995)

Abstract—The wave energy devices currently in operation in the United Kingdom and India and those that are to be built in Europe are based on the principle of the oscillating water–air column. In these devices the pneumatic energy of the oscillating air column is converted to mechanical energy of rotation by a Wells turbine. A monoplane (single plane) Wells turbine can absorb only a certain maximum pneumatic pressure amplitude due to tip speed limitations. For wave energy devices which produce large amplitudes of pneumatic pressure a biplane Wells turbine with or without guide vanes can be used. The prediction methods currently available and parameters controlling the aerodynamic performance of the Wells turbines are reviewed. Some novel techniques to improve the performance of Wells turbine are suggested.

CONTENTS

NOMENCLATURE

A_b—blade planform area lc
AR—blade aspect ration l/c
c—blade chord length
C_l—lift coefficient $L/(1/2\rho w^2 c)$
C_d—drag coefficient $D/(1/2\rho w^2 c)$
C_x—axial force coefficient $F_x(1/2\rho w^2 c)$
C_θ—circumferential force coefficient $F_\theta/(1/2\rho w^2 c)$
D—drag force on the blades
D_h—turbine hub diameter
D_t—turbine tip diameter
F_θ—force in the circumferential direction
F_x—force in the axial direction
f—frequency of air flow
G—gap between the planes of a biplane turbine

g—blade offset
h—hub to tip ratio D_h/D_t
KE*—normalised kinetic energy $(1/2\rho V^2/\Delta p)$
L—lift force on blades
M—Mach number relative to blades w/c
N—number of blades
Δp—pressure drop across the rotor
p^*—non-dimensional pressure drop $\Delta p/(\rho w^2 D_t^2)$
P_o—total pressure
Q—flow rate
R—Reynolds number $\rho wc/\mu$
T—cyclic period
Tu—turbulence level at inlet to turbine
U—blade circumferential velocity
u—induced velocity in the direction of circumferential velocity
w—relative velocity
V_x—axial velocity
V_T—total velocity $(V_x^2 + V_\theta^2)^{1/2}$
V_θ—component of absolute velocity in direction of circumferential velocity
W_o—power output
W_T—power input
σ—turbine solidity $2Nc/[\pi D_t(1 + h)]$
ρ—density
ω—angular velocity
ϕ—flow ratio V_x/U_t
η—aerodynamic efficiency W_0/W_I
η_b—blade element efficiency
α—blade incidence flow angle
β—angle of absolute velocity
Γ—circulation around an aerofoil
γ—exit circulation, $\pi D_t V_\theta$
θ—angle defining relative circumferential position of blades in the two planes of a biplane turbine, see Fig. 4
Ω—flow rotation
τ—blade thickness ratio
τ_c—blade clearance at tip

Subscripts
1—inlet to plane 1
2—outlet to plane 1
3—outlet of plane 2
0—single aerofoil
h—hub
t—tip

Superscript
time average

1. INTRODUCTION

Wave energy is an alternative form of energy which is pollutant free and in the near future likely to be economically viable. For countries surrounded by the sea such as the British Isles, Japan, India, and Portugal, to mention a few, and remotely situated island communities, wave energy conversion is an attractive proposition. The United Kingdom took a lead in harnessing wave power about a decade ago through nationally co-ordinated research activities at several establishments, one of which was Queen's University, Belfast (QUB). Of the several wave energy devices investigated, the devices based on the principle of an oscillating water column have been found to be the most practicable for wave energy conversion.[57–59] The QUB device now installed at Islay in Scotland (Fig. 1) uses such a principle where the hydraulic energy of oscillating wave motion is converted to an oscillating air column in a chamber called the device. The energy from this bi-directional air flow is converted to mechanical energy of rotation by an air turbine invented by A. A. Wells, known as the Wells turbine[24] (Fig. 2). The power conversion chain is illustrated in Fig. 3. For efficient performance of a wave energy system it is essential that the turbine is matched with the device for the pressure drop for a wide range of flow rates. The pressure drop across a mono plane (single plane) Wells turbine is proportional to the square of the rotor tip Mach number and has a limit if transonic flow effects on the blades are to be avoided. Therefore for devices which are designed to absorb wave amplitudes (pressures) considerably larger than that limited by the tip speed of a single plane Wells turbine a multiplane[27] (Fig. 4) (without guide vanes) or multistage[8] (with guide vanes) Wells turbine can be used. The Wells turbine installed in the wave energy device at Islay in Scotland[43, 58] is a biplane Wells turbine whereas the one installed in the device at Trivandrum in India[23,49] is a monoplane Wells turbine, the designs of which were based on small-scale experiments and semi-empirical theories. There are plans to build three new wave power stations in Europe with a Wells turbine in the power conversion chain.

This paper presents the present state of knowledge on this turbine. The prediction methods currently available and the variables which affect the aerodynamic performance of a Wells turbine are discussed in this paper. The review is divided into eight sections. The principle of the Wells turbine is introduced in Section 2. The prediction methods available are discussed in Section 3. This section also contain some information on aerofoils in cascade of 90 degrees stagger angle. Section 4 describes the various factors controlling the

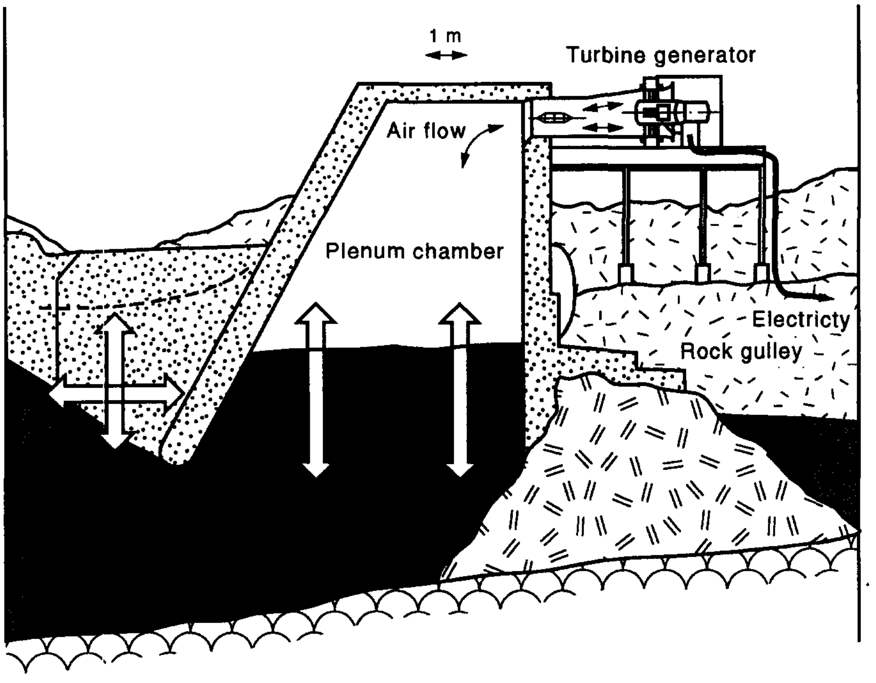

Fig. 1. A schematic diagram of Queen's University of Belfast Wave Energy device at Islay in Scotland.

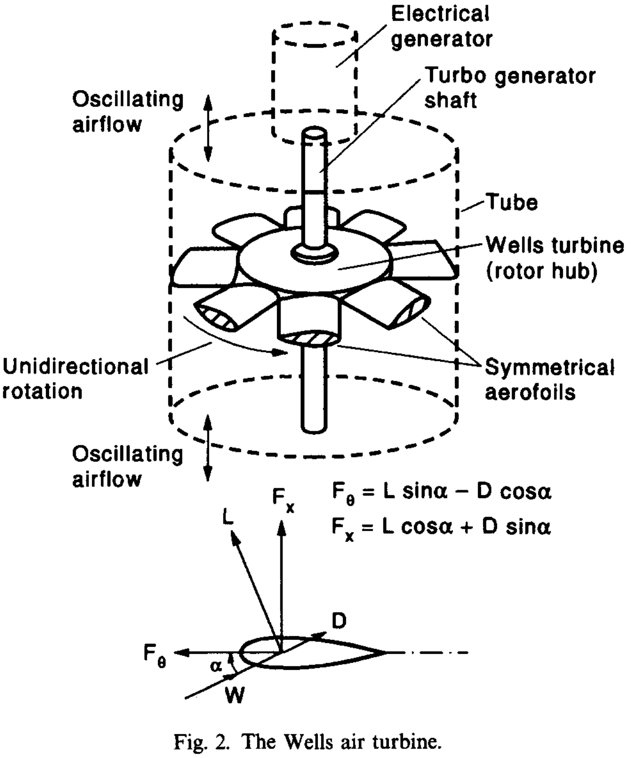

Fig. 2. The Wells air turbine.

aerodynamic performance of the Wells turbine. The concept of biplane Wells turbine and the performance of such a turbine is given in Section 5. The starting performance of a Wells turbine is explained in Section 6. Some methods for improving the performance of a Wells turbine are outlined in Section 7. Section 8 contains some concluding remarks.

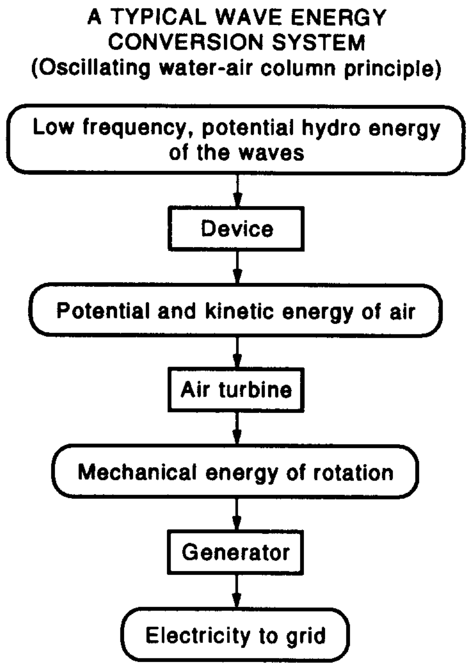

Fig. 3. The power conversion chain in an oscillating water column wave energy system.

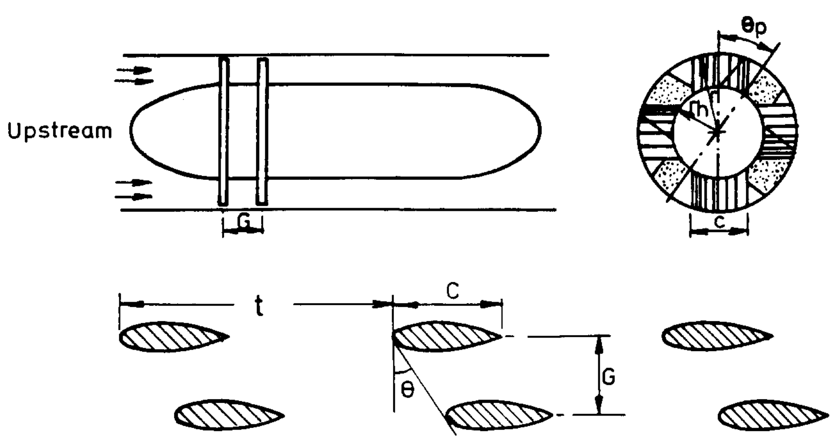

Fig. 4. The biplane Wells turbine.

2. THE PRINCIPLE OF THE WELLS TURBINE

In its simplest form the Wells air turbine rotor consists of several symmetrical aerofoil blades positioned around a hub with their chord planes normal to the axis of rotation[24, 26, 30, 60] (Fig. 2). The turbine may have guide vanes on both sides of the rotor.[6, 54] According to the classical aerofoil theory, an aerofoil which is set at an angle of incidence, α, in a fluid flow, generates a lift force, L, normal to the free stream. The aerofoil also experiences a drag force, D, in the direction of the free stream (relative velocity). These lift and drag forces can be resolved into tangential (in the plane of rotation) and axial (normal to the plane of rotation) components F_θ and F_x respectively. The effects of flow incidence on the tangential and axial force coefficients C_θ and C_x for a two dimensional aerofoil are shown in Fig. 5a, b respectively.[30] Results shown here are for two dimensional NACA12, NACA15, NACA18, NACA21 aerofoils at several Reynolds numbers and are based on

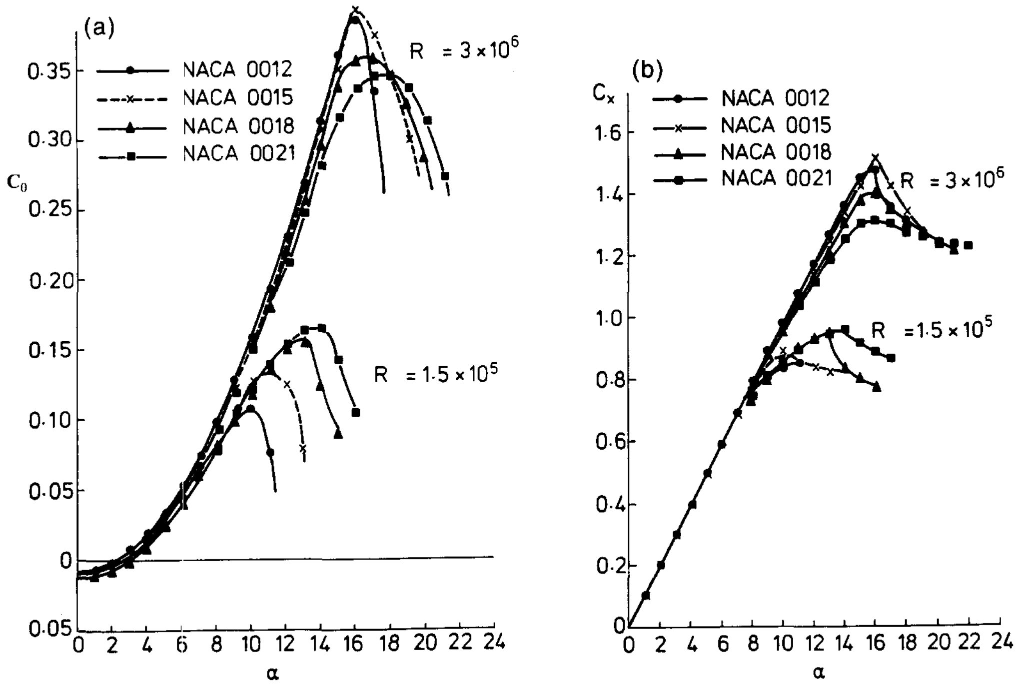

Fig. 5. Aerodynamic forces on two dimensional NACA aerofoils. (a) Variation of peripheral force coefficient with incidence angle. (b) Variation of axial (normal) force coefficient with incidence angle.

available wind tunnel data for lift and drag coefficients for such aerofoils. For a Wells turbine in a bi-directional airflow the airflow incidence angle changes sign depending on the direction. If α can be regarded as positive when the airflow is in one direction it is negative when the airflow is in the opposite direction. For a symmetrical aerofoil, the direction of tangential force F_θ is the same for both positive and negative values of α. If such aerofoil blades are positioned around an axis of rotation, they will always rotate in a single direction regardless of the direction of airflow. Therefore the turbine does not need rectifying valves in a bi-directional airflow. It is because of this unique feature that the Wells turbine is well suited for wave energy conversion from devices based on the principle of oscillating water column.

The aerodynamic performance of a Wells turbine can be typified[33] by the variation of non-dimensional pressure drop p^* and aerodynamic efficiency η with flow ratio ϕ as shown in Fig. 6. The results shown here are for a mono-plane turbine at two values of solidity σ and also for a bi-plane turbine. For a given rotational speed there is a linear relationship between pressure drop and flow rate (Fig. 6a) and this is essential for matching the turbine with an oscillating water column wave energy device which also has a similar characteristic. The turbine has nearly the same efficiency (Fig. 6b) over a wide range of flow rates. The pressure drop produced can be increased by increasing the solidity for a mono-plane turbine or by using a bi-plane turbine. At low flow rates (small airflow incidences) the component of drag in the chordwise direction is larger than that of the lift and therefore the efficiencies are negative. At these incidences the pneumatic power input is dissipated as heat and there is no power output. It should be noted that under these conditions the Wells turbine unlike conventional turbines does not act as a pump. At large flow rates (large incidences) the boundary layer on the blades tend to separate (stall) leading to a drop in efficiency. In a bi-directional air flow the Wells turbine can be designed to operate over a incidence range $\pm\alpha_{max}$ where α_{max} is less than α_s, and where α_s is the stall incidence. In a bi-directional and random airflow the turbine blades will experience time varying torque which can be smoothed by a high inertia flywheel/rotor. It can be shown that for a given

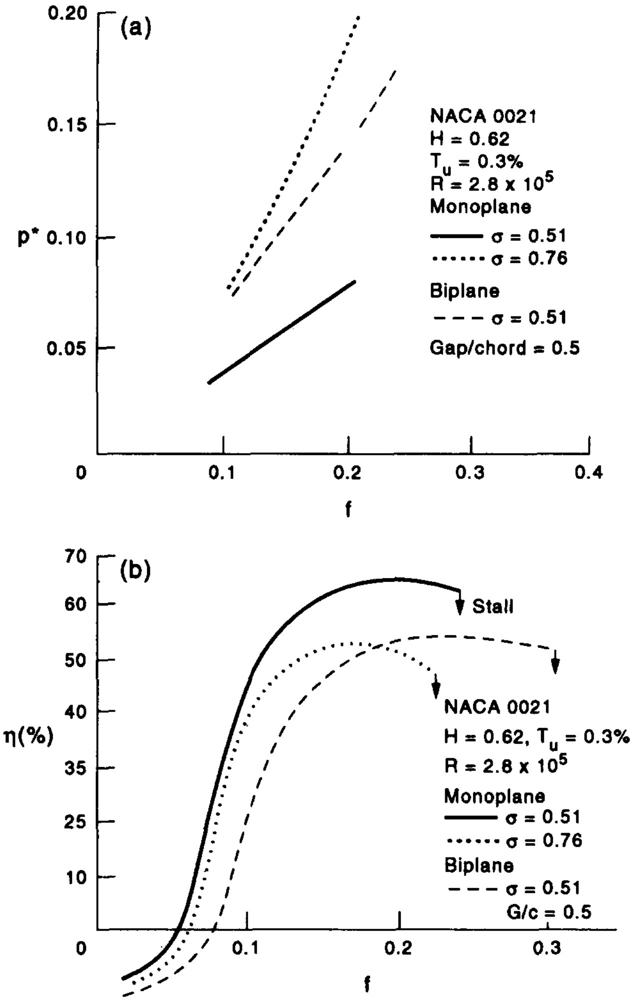

Fig. 6. Typical performance curves for a Wells turbine. (a) Pressure drop–flow ratio relationship. (b) Aerodynamic efficiency–flow ratio relationship.

turbine speed if the variation of airflow velocities with time is sinusoidal the power lost due to energy dissipation by the turbine at small incidences forms only a small part of a time averaged power output. This may not be the case for a turbine in random airflow where the turbine blades may experience small incidences over significant periods and the time averaged efficiency over a long period of time may be 5 to 10% lower than the peak efficiency.

Within this range of operational incidence angles the component of lift force forms a significant part of the axial force which explains almost a linear relationship between axial force coefficient and flow incidence angle (Fig. 5a). In a bi-directional airflow the axial forces will vary with time and will have a directional change every half a cycle. Such dynamic axial thrust forces will have to be borne by suitable bearings or can be virtually eliminated by splitting the airflow[7] as shown in Fig. 7.

3. PREDICTION METHODS

The methods generally used for the prediction of performance of axial flow machines have been used to study the aerodynamic performance of the Wells turbine. These include both a radial equilibrium approach and actuator disc theory.[2, 9, 19] In applying these

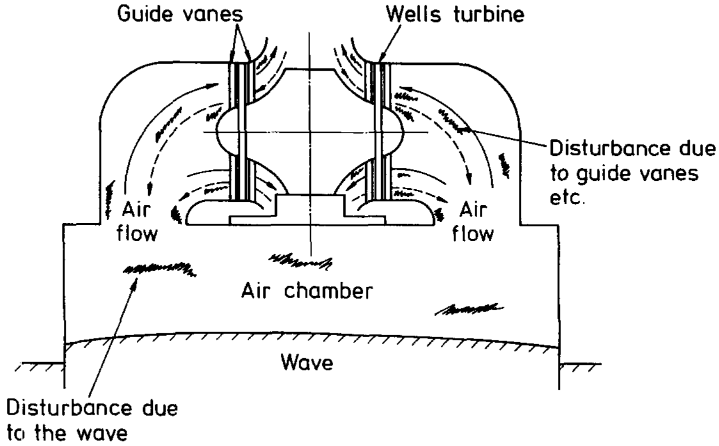

Fig. 7. A scheme for alleviating axial thrust produced by the Wells turbine.

methods to predict the Wells turbine performance the flow in the rotor is divided into several annular rings and each ring is treated as a two-dimensional cascade with the blade stagger angle 90°. Since the frequency of oscillating airflow in a wave energy device is typically less than 0.1 Hz, the flow through the rotor can be assumed to be quasi-steady. Methods for analysing the flow in a cascade of 90 degrees stagger angle, the radial equilibrium theory applied to both the stationary guide vanes and the rotor, and the concept of actuator disc theory are outlined in the following sections.

3.1. AEROFOILS IN A TWO DIMENSIONAL CASCADE OF 90° STAGGER ANGLE

The performance of a monoplane (single plane) rotor is affected by mutual aerodynamic interference between the blades. The mutual interference is due to velocities induced by the blades on each other (inviscid effects) and the wakes produced by the blades (viscous effects). This interference is a function of airflow incidence and blades gap to chord ratio (solidity). The mutual interference effects for aerofoils in cascade of stagger angle $\pi/2$ can be understood by replacing the aerofoils by a series of vortex singularities of strength Γ at quarter chord position as shown in Fig. 8a. The induced velocities on an aerofoil, normal to the chord line near the leading and trailing edges (v) and parallel to the chord line above the upper and below the lower surfaces (u), due to the presence of aerofoils upstream (us) and downstream (ds) are shown in this figure. The upwash and downwash effect on the flow around an aerofoil due to the neighbouring aerofoil would cause the effective angle of incidence to decrease near the leading edge and increase near the trailing edge of the aerofoil. This should reduce the relative differences in aerodynamic loading between the leading edge and trailing edge. Of more significance, however, is the fact that the circulation and lift on the aerofoil are increased as a result of the increase in velocities above and decrease below the aerofoil due to the presence of the neighbouring aerofoils. The effect of these induced velocities on the pressure distribution for a NACA0012 aerofoil for several solidity (chord-to-pitch ratios) can be observed from Fig. 8b. The results shown here are predicted values[55] based on a method of singularities[19] also known as Mortenson method. Simulation in a wind tunnel of cascade of infinite number of aerofoils at a stagger angle of $\pi/2$ is practically impossible. However, the measured pressure distributions[37] on an aerofoil in a cascade of such a stagger but with a finite number of blades (Fig. 8c) qualitatively support the predictions.

A simple method of evaluating the interference effects is that based on a potential flow analysis of flat plate aerofoils in a cascade by Weinig.[56] According to his analysis the value

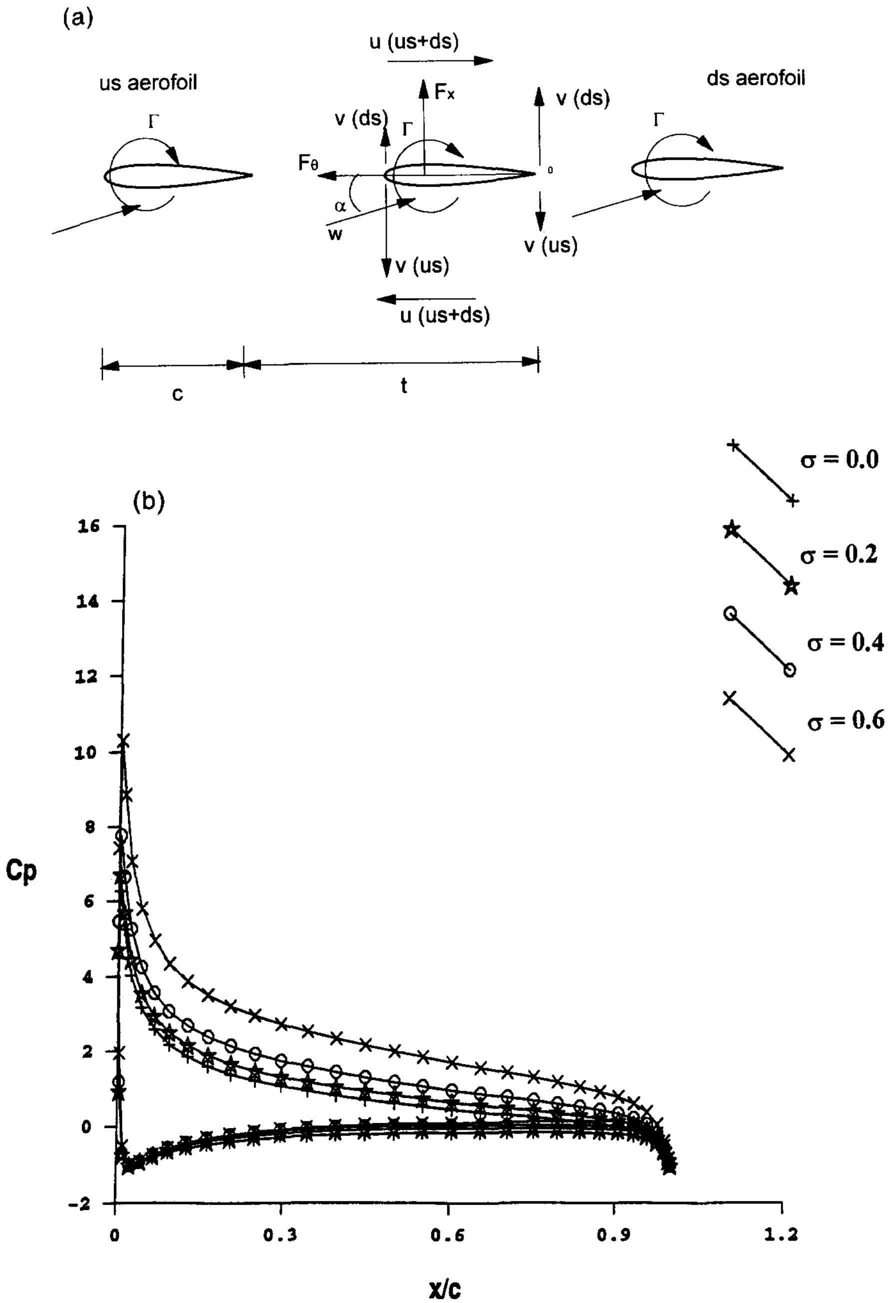

Fig. 8a, b

of C_l for an aerofoil in a cascade can be corrected for cascade effects by a factor k such that,

$$C_l = kC_{l_0}$$

where, C_{l_0} refers to lift coefficient for an isolated flat plate aerofoil and factor m for a cascade of stagger angle of $\pi/2$ is given by

$$k = (2t/\pi c)\tan(\pi c/2t)$$

where, c is the chord length and t is the pitch.

A similar correction could be applied to the lift for aerofoils of finite thickness in a cascade. As drag cannot be predicted by the potential flow analysis one has to assume that

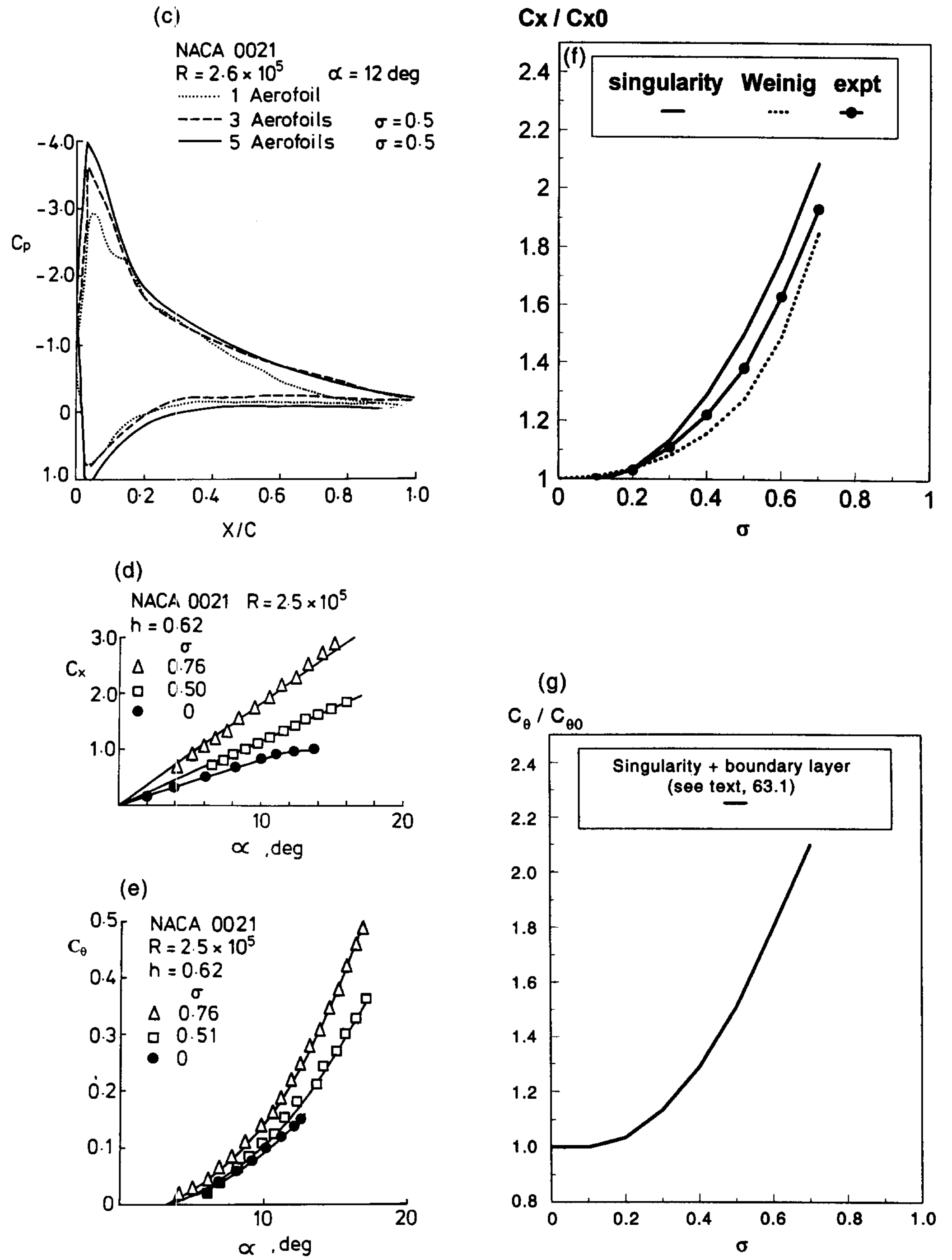

Fig. 8. Aerodynamics of a monoplane cascade at a stagger angle of $\pi/2$. (a) Mutual interference between the aerofoils due to bound vortices, us and ds refers to upstream and downstream aerofoils. (b) Effect of solidity on the pressure distribution on an aerofoil. (c) Measured Pressure Distributions in a wind tunnel with finite number of blades. (d) Calculated values of axial force coefficients from the Wells turbine and wind tunnel tests. (e) Calculated values of peripheral force coefficients from the Wells turbine and wind tunnel tests. (f) A comparison of predictions with experimental data for axial force coefficients. (g) Prediction for peripheral force coefficients.

$C_d = C_{d0}$. Such a procedure has been used[3] in the prediction of the Wells turbine performance.

Another approach to evaluate the mutual interference effects between the aerofoil blades is by an analysis where the surface of aerofoils in a cascade are replaced by singularities[45] as mentioned earlier. This method also being a potential flow method can predict only lift and not drag values. The drag can be calculated by a boundary layer analysis using the pressure distribution obtained by the potential flow method. Aerofoils in a cascade at an incidence have an equivalent incidence α_{eq} that produces approximately same pressure distributions on the upper surface as that of an isolated aerofoil at an incidence α. It is suggested[30,54] that both C_θ and C_x for an aerofoil in a cascade can be evaluated by a simple proportional formula

$$\frac{C_\theta}{C_{\theta 0}} = \frac{C_x}{C_{x0}} = \left[\frac{C_x}{C_{x0}}\right]_{\text{pred}}$$

where, $C_{\theta 0}$ and C_{x0} are measured values, in a wind tunnel, of force coefficients on an isolated aerofoil at an equivalent incidence, α_{eq}. $[C_x/C_{x0}]_{\text{pred}}$ is the ratio of the predicted normal aerodynamic force on an aerofoil in a cascade to that of an isolated aerofoil at an incidence as calculated by the potential flow methods. Such procedures have been used[30,52] in predicting the performance of the Wells turbine.

A third approach for the prediction of mutual interference effects on an aerofoil in a cascade of stagger angle of $\pi/2$ is a semi-empirical approach[37] based on a correlation between calculated values of mean aerodynamic force coefficients from Wells turbine tests and two-dimensional aerofoil data from wind tunnels. In this approach the axial force F_x and the power output W_0 for a Wells turbine at a given solidity and Reynolds number can be expressed in terms of mean aerodynamic force coefficients for the blades as

$$F_x = \frac{1}{2} N C_x \rho w^2 A_b$$

$$W_0 = \frac{1}{2} N C_\theta \rho W^2 A_b U \ .$$

The pressure drop across the rotor can be expressed in terms of the axial force on the blades as:

$$F_x = \Delta p A_a$$

efficiency can be expressed as,

$$\eta = \frac{C_\theta}{C_x}\left(\frac{1}{\phi}\right).$$

Typical results[37] for the variation of C_x and C_θ with mean airflow incidence to the blades α ($\tan^{-1}\phi$) based on Wells turbine tests in an uni-directional air flow are shown in Fig. 8d and e respectively. The results shown here are for a turbine with NACA 0021 blade, $h = 0.62$, $R = 2.5 \times 10^5$, and $\sigma = 0.5$ and 0.76. Also shown in these figures are the results of two-dimensional wind-tunnel tests of isolated aerofoils ($\sigma = 0$). Both the turbine and wind-tunnel results show a linear variation of C_x with α (Fig. 8d) for incidences up to stall angle. The C_θ versus α (Fig. 8e) curves are non-linear and for small angles of incidence the values of C_θ are negative. It is observed from these figures that at any given airflow incidence, the aerodynamic forces increased with turbine solidity.

The normalised values C_x/C_{x0} and $C_\theta/C_{\theta 0}$ based on the prediction methods[57] and experimental data from turbine tests[10,11,30,34,53,55] plotted against solidity σ are shown in Fig. 8f. A plot of $C_\theta/C_{\theta 0}$ vs σ based on the method of singularities for lift and drag obtained by boundary layer calculations based on pressure distributions predicted by the singularity method is shown in Fig. 8g. The two-dimensional aerofoil data at a corresponding Reynolds number for these calculations were obtained from available wind tunnel data.[16,35] Relative to experimental data (Fig. 8e) the predictions based on the method of singularities over estimate and that based on the method of Weinig underestimate the axial force coefficients. Considering that the data are taken from several experimental rigs, the correlation between (C_x/C_{x0}) and σ, within the range of test Reynolds number, is reasonable. This correlation can be expressed as,

$$C_x/C_{x0} = 1/(1-\sigma^2)\,.$$

It is observed from Fig. 8f that the effect of solidity on $C_\theta/C_{\theta 0}$ is similar to that on C_x/C_{x0} both in magnitude and trend. These results suggest that the aerodynamic forces on the blades increase considerably with solidity and that the aerodynamic efficiency of the blades, which is proportional to the ratio of peripheral force to axial force, does not change appreciably with solidity.

3.2. RADIAL EQUILIBRIUM THEORY

According to radial equilibrium theory[2,9] the flow is assumed to be irrotational, axisymmetric and the radial component of velocity V_r is assumed to be negligible everywhere in the flow field except within the blade rows (Fig. 9) i.e. $V_r = 0$. It can be shown from the momentum equation in radial direction, that for the radial equilibrium to exist the pressure force in the radial direction must balance the centripetal acceleration i.e.

$$\frac{V_\theta^2}{r} = \frac{1}{\rho}\frac{\partial p}{\partial r}\,. \tag{1}$$

A particular case of radial equilibrium is that axial velocity V_x remains constant in the flow field and circulation is constant along the radius which implies that blades shed no vorticity and the specific work done on a blade is invariant with radius.

3.2.1. *Radial Equilibrium at the Inlet of the Rotor*

Consider a row of stationary guide vanes upstream of a rotor (Fig. 10). If the flow through the guide vanes is assumed to be inviscid and irrotational then

$$P_{01} = P_1 + \frac{\rho}{2}(V_{x1}^2 + V_{\theta 1}^2) = \text{cons}\tan t \tag{2}$$

$$\Omega_{\theta 1} = \frac{\partial V_{r1}}{\partial x} - \frac{\partial V_{x1}}{\partial r} = 0 \tag{3}$$

and from Eqs (1), (2) and (3) it can be shown that

$$\tan\beta_1 = \frac{V_{x1}}{V_{\theta 1}} = k_1 r \tag{4}$$

where, k_1 is a constant

$$\text{and } \gamma_1 = \text{const.} \tag{5}$$

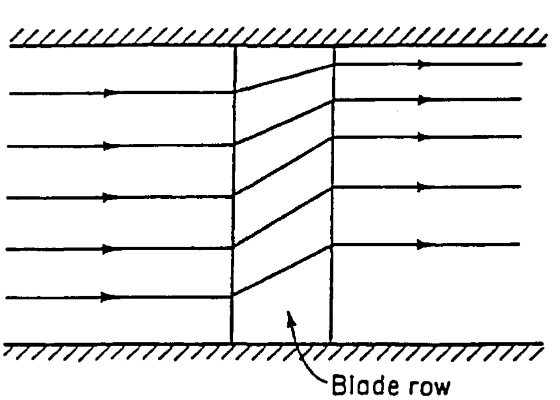

Fig. 9. The concept of radial equilibrium. The blade row represents the turbine.

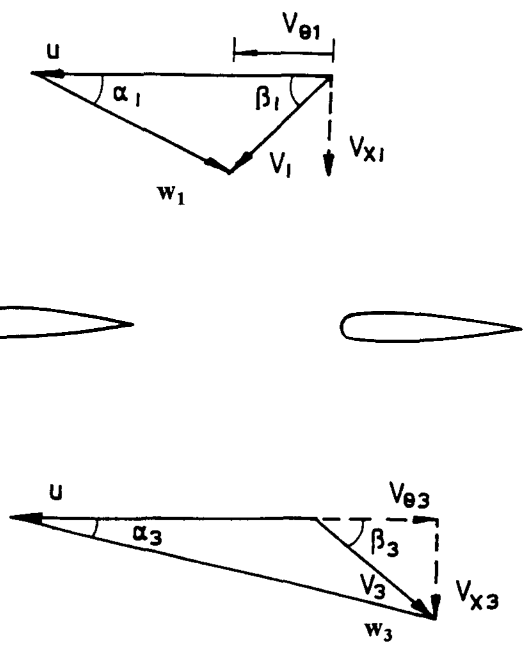

Fig. 10. Velocity triangles for a monoplane rotor with inlet guide vanes.

Equations (4) or (5) can be used to design inlet guide vanes with radial equilibrium at the exit of the guide vanes (inlet of the rotor).

3.3. THE WELLS TURBINE PERFORMANCE CALCULATIONS

From the velocity triangle at the inlet of the rotor (Fig. 10) the variation of flow incidence to the blades with radius is given by

$$\cot\alpha_1 = U/V_{x1} - \cot\beta_1 \tag{6}$$

where $U = \omega r$ is the blade peripheral velocity of the rotor and the relative velocity W_1 and circumferential velocity $V_{\theta 1}$ of the airflow is given by

$$\begin{aligned} w_1 &= V_{x1}/\sin\alpha_1 \\ V_{\theta 1} &= V_{x1}/\tan\beta_1 \, . \end{aligned} \tag{7}$$

For inlet flow with no guide vanes $\beta_1 = \pi/2$.
In an annular ring of area $2\pi r\,\mathrm{d}r$ the power output from rotor is given by

$$dW_0 = N\,\mathrm{d}F_\theta U \tag{8}$$

where

$$\mathrm{d}F_\theta = 1/2C_\mathrm{T}\rho w_1^2 c\,\mathrm{d}r\,. \tag{9}$$

The axial force on the blades in the annulus is $N\,\mathrm{d}F_x$
where,

$$\mathrm{d}F_x = 1/2C_x\rho w_1^2 c\,\mathrm{d}r \tag{10}$$

where C_θ and C_x are chordwise and normal force coefficients and are dependent on C_1 and C_d which in turn are functions of several parameters such as blade chord Reynolds number, Mach number, rotor solidity, hub-to-tip ratio and tip clearance.

The axial force is balanced by the pressure force on the rotor resulting in

$$\frac{p_1 - p_2}{(1/2)\rho V_{xi}^2} = \frac{NC_x c}{2\pi r \sin^2 \alpha_1} \tag{11}$$

If the kinetic energy at the exit of the rotor is considered as a loss (some of the kinetic energy can be recovered by the exit guide vanes) the power input to the rotor is

$$\mathrm{d}W_I = (P_{01} - P_{02})\,\mathrm{d}Q \tag{12}$$

where

$$\mathrm{d}Q = V_{x1} 2\pi r\,\mathrm{d}r. \tag{13}$$

The blade element efficiency is

$$\eta_b = \frac{\mathrm{d}W_0}{\mathrm{d}W_I}. \tag{14}$$

The radially averaged aerodynamic efficiency

$$\eta = \int_{\mathrm{rhub}}^{\mathrm{rtip}} \mathrm{d}W_0 \Big/ \int_{\mathrm{rhub}}^{\mathrm{rtip}} \mathrm{d}W_I. \tag{15}$$

Equating the torque on the blade element to change in angular momentum results in

$$\gamma_1 - \gamma_2 = \frac{V_{x1} N C_\theta c}{2 \sin^2 \alpha}. \tag{16}$$

The drag force on the cascade of blades in the annulus and the viscous losses are given by

$$\mathrm{d}F_D = 1/2 N C_d \rho w_1^2 c\,\mathrm{d}r \tag{17}$$

and the energy dissipation due to viscous effects on the blades is given by

$$\mathrm{d}E_D = \mathrm{d}F_D w_1\,. \tag{18}$$

For energy balance

$$(P_{01} - P_{02}) 2\pi r\,\mathrm{d}r\, V_{x1} = \mathrm{d}E_D + \mathrm{d}W_0 \tag{19}$$

from which the stagnation pressure drop Δp_0 can be expressed as

$$\Delta p_0 = \frac{N c \rho w_1^2}{4\pi r}\left[\frac{C_D}{\mathrm{Sin}\,\alpha_1} + C_T(\cot\alpha_1 + \cot\beta_1)\right] \tag{20}$$

The kinetic energy of air at the exit of the rotor in the annulus is given by

$$\mathrm{d}E_k = \rho\,\mathrm{d}Q V_2^2/2. \tag{21}$$

The aerodynamic efficiency can also be expressed as

$$\eta = \frac{\int_{\mathrm{hub}}^{\mathrm{tip}} \mathrm{d}W_0}{\int_{\mathrm{hub}}^{\mathrm{tip}} (\mathrm{d}W_0 + \mathrm{d}E_d + \mathrm{d}E_k)}. \tag{22}$$

The effect of tip clearance using the methods used in turbomachines(21) and compressibility effects using Prandtl–Glauert rule could be included in the above analysis.(30, 31)

3.4. RADIAL EQUILIBRIUM

In general different streamlines in the rotor may be subjected to different amounts of energy transfer and the total pressure downstream of the rotor

$$P_{02} = P_{02}(r) = p_2 + \frac{\rho}{2}(V_{x2}^2 + V_{T2}^2). \tag{23}$$

With radial equilibrium downstream of the rotor the above equation can be written as

$$\frac{d}{dr}(V_{x2})^2 + \frac{1}{r^2}\frac{d}{dr}(rV_{T2})^2 = \frac{2}{\rho}\frac{dP_{02}}{dr} \tag{24}$$

if, P_0 = constant
the above equation reduces to

$$\frac{d}{dr}(V_{x2}^2) = -\frac{1}{4\pi^2 r^2}\gamma_2^2 \tag{25}$$

from which $V_{x2} = V_{x2}(r)$ can be determined.
For a case where

$$\frac{dP_{02}}{dr} = 0, \text{ and } \gamma_2 = \text{constant}$$

the above equation simplifies to V_{x2} = constant.

3.5. ACTUATOR DISC THEORY

Experiments on axial flow machines have shown that there is a considerable redistribution of mass flow in the region outside the blade rows and that radial velocities must exist outside this region. This leads to the development of actuator disc theory[2,9] in which each blade row is represented by a discontinuity in flow (Fig. 11) parameters. Further to the assumptions that the flow is steady, and axisymmetric, it is assumed that vorticity everywhere is small and stagnation pressure is nearly constant.

Further, the variation of circumferential vorticity Ω_θ and velocity V_θ is assumed to be invariant with axial direction.

If u_r, U_T and u_x are small radial, tangential and axial velocity, respectively, and are superimposed on the radial equilibrium values and exist only in the neighbourhood of the blades such that the total velocities are

$$\begin{aligned} v_r &= u_r \\ v_\theta &= V_\theta + u_r \\ v_x &= V_x + u_x \end{aligned} \tag{26}$$

where, V_θ and V_x are radial equilibrium values ($V_r = 0$).
It can be shown with the assumptions mentioned earlier that the velocities upstream and

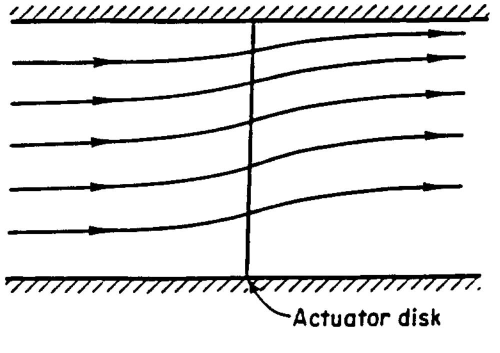

Fig. 11. The concept of actuator disc, the blade row is represented by a discontinuity.

downstream of the rotor can be expressed as

$$\begin{aligned} v_{x1} &= V_{x1} + u_{x1} \\ v_{x2} &= V_{x2} + u_{x2} \\ u_{x1} &= -u_{x2} = \left(\frac{V_{x2} - V_{x1}}{2}\right) e^{-\pi X/b} \end{aligned} \tag{27}$$

where, V_{x1} and V_{x2} are the axial velocity based on radial equilibrium and b is the blade height.
At the blade row (disc) itself ($x = 0$) the above equation simplifies to

$$v_{x1} = v_{x2} = \frac{V_{x1} + V_{x2}}{2} \,. \tag{28}$$

With the calculated values of V_{x1} and V_{x2} by radial equilibrium theory and velocities v_{x1} and v_{x2} calculated from actuator disc theory the performance calculations can be reworked by an interactive procedure.

3.6. THE GUIDE VANE ANGLES

The required variation of inlet guide vane angles with radius for radial equilibrium of flow at the inlet of the rotor was given in Section 3.2. Methods for calculating the inlet and outlet guide vane angles as a function of rotor performance are given below.

A simple approach to guide vane design is based on inlet and outlet flow angles for a potential flow on a flat plate cascade. For such a cascade as described in Section 3.1, the lift coefficient C_L for the cascade can be expressed as

$$C_l = C_{l0} \frac{2t}{\pi c} \tan\left(\frac{\pi c}{2t}\right) \tag{29}$$

and

$$C_\theta = C_l \sin\alpha \,. \tag{30}$$

For a flat plate $C_{l0} = 2\pi \sin\alpha$.

Equating the chordwise force on the blades to the change of momentum in that direction results in[4]

$$\cot\beta_2 = \cot\beta_1 + 2\tan\left(\frac{\pi c}{2t}\right) \tag{31}$$

where β_1 and β_2 are inlet and outlet flow angles (Fig. 10). For a Wells rotor in an oscillating airflow the guide vanes have to be symmetrical such that $\beta_2 = \pi - \beta_1$ resulting in $\beta_1 = (\pi/2) \times (1 + c/t)$ which indicates that the guide vane angles are only a function of rotor solidity. Such an analysis is not accurate because the drag which is neglected in the analysis contributes significantly to chordwise force and should have a considerable effect on the guide vane angles. A more accurate method of calculating guide vane angles is to use the Eq (16) given in Section 3.3 given by

$$\gamma_1 - \gamma_2 = (V_{x1} N c C_\theta)/(2\sin^2\alpha)$$

which takes into consideration the drag coefficient in the calculations. The above equation can be expressed as in

$$\cot\beta_1 - \cot\beta_2 = \frac{N c C_\theta}{4\pi r \sin^2\alpha_1} \tag{32}$$

where α_1 and β_1 are related (from inlet velocity triangle) by

$$\cot\alpha_1 + \cot\beta_1 = \frac{u}{V_{x1}} = \frac{\omega r}{V_{x1}} \,. \tag{33}$$

For a given geometry, speed and flow rate a prescribed distribution of β_1 as a function of r would result in a distribution of α_1 (equation) which in turn leads to a certain C_θ distribution as a function of r. The required symmetry of guide vanes that $\beta_2 = \pi - \beta_1$ may be satisfied only for a certain flow rate. The inlet guide vane angles could be prescribed such that variation of β_1 with radius satisfies the condition that γ_1 = constant or any other type of variation with r.

3.7. COMPARISON OF PREDICTIONS WITH EXPERIMENTS

The performance of the Wells turbine based on the prediction methods given in Sections 3.1–3.6 are discussed in this section. The predictions are also compared with some of the experimental results from small-scale Wells turbine test rigs in which the flows were unidirectional.

The aerodynamic performance of a monoplane Wells turbine as based on predictions is compared with experiments in Figs 12–16. The experimental results are from unidirectional flow test rigs 0.2 m and 0.6 m diameters. Figures 12–13 refer to results of 0.2 m diameter turbine whereas Figs 14–16 refer to 0.6 m diameter turbine.

It should be mentioned that experimental data from small-scale tests are subjected to errors typically of the order of $\pm 5\%$. This is largely due to the fact that the bearing and friction losses are a significant fraction of the output power and the estimation of these losses is subject to uncertainty. Nevertheless there is a reasonable agreement between experiments and the prediction based on radial equilibrium for pressure (Fig. 12a), and efficiency (Fig. 12b) for a small-scale turbine.

For a given rotor speed the non-dimensional value of p^* is proportional to the pressure drop Δp and the flow coefficient ϕ is proportional to the flow rate Q. Figure 12a shows that for a given solidity there exists, except at relatively small flow rates, a linear relationship between pressure drop and flow rate. This unique feature of the Wells turbine makes it possible to match the turbine with a wave energy device of oscillating water–air column which also has similar pressure drop-flow rate characteristics. This is only to be expected as the pressure drop is largely governed by the lift coefficient of the blade. For incidences less than stall angle α is proportional to flow coefficient ϕ and C_L is proportional to α. It is also noticeable from Fig. 12a that for a given flow coefficient the pressure drop increases with the solidity of the turbine. Therefore a solidity can be selected to match the available pressure drop. For wave energy devices with relatively large pressure amplitudes it may be appropriate to use a biplane turbine (see Section 5). The $\eta - \phi$ curves (Fig. 12b) show that the efficiency of the turbine increases with ϕ up to a certain value after which it decreases rapidly due to boundary layer separation on the blades. The peak efficiency of the 0.2 m diameter rotor is rather low ($\sim 50\%$) because of small blade chord Reynolds numbers ($\sim 2.5 \times 10^5$) under which these tests were conducted. It is also noticeable that the efficiencies decrease with the increase in turbine solidity and this is due to an increase in kinetic energy losses associated with swirl. A comparison of measured values with predictions of pressure drops at several radii (Figs 13 and 14) indicate that the assumption of radial equilibrium for pressure is reasonably valid. For a Wells turbine rotor with small or moderate solidity, the effect of solidity on the aerodynamic force coefficients is small (Figs 8f and 8g) and for a rotor at constant speed and a blade profile with constant thickness ratio along the chord, the normal force coefficient $C_x \propto \alpha$

and,
$$\sin\alpha \approx \alpha \approx \tan\alpha = \frac{V_x}{\omega r} \propto \frac{1}{r}$$

and from Eq. (11),
$$\Delta p \propto c$$

so that for a rotor with constant chord the pressure drop across the rotor is approximately constant with the radius. This may not be the case for a rotor of high solidity or a rotor wherein the chord length varies with radius.

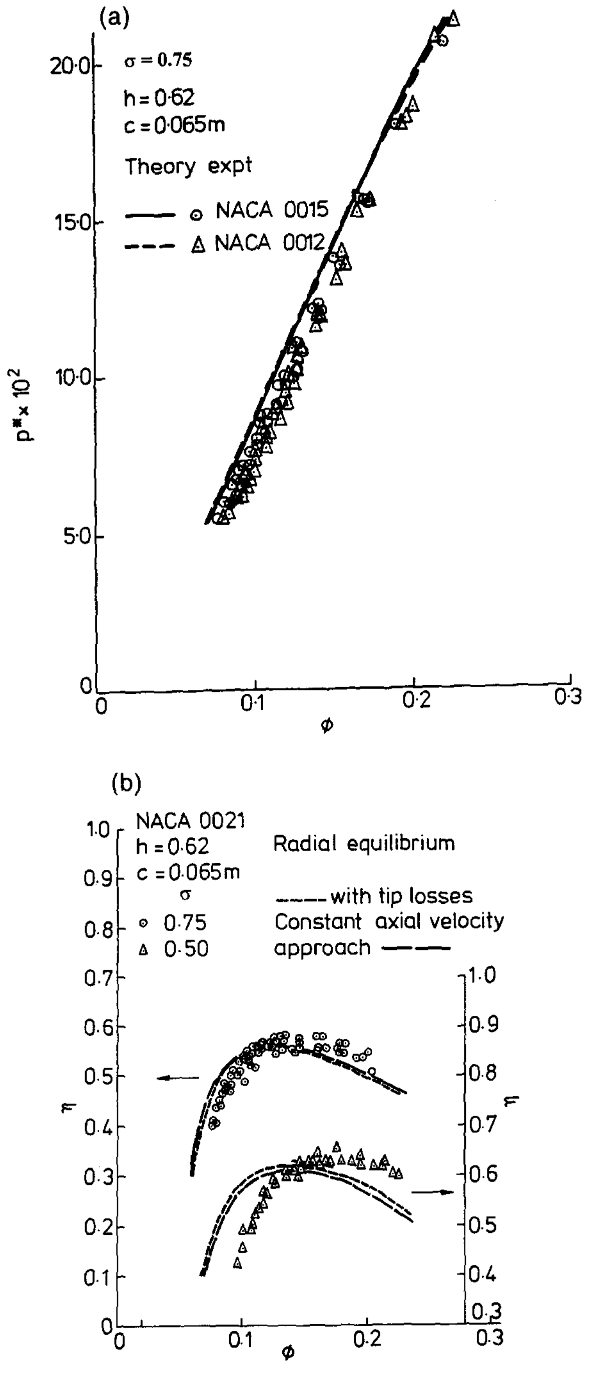

Fig. 12. Comparison of prediction with experiments for a small scale (0.2 m diameter) Wells turbine. (a) Pressure drop. (b) Efficiency—considering with and without tip losses.

Experiments[30] and predictions[4] of axial velocities upstream and downstream of the rotor (Fig. 14) show that the axial velocities vary with radius and the variation of axial velocities in the plane of the rotor is large for a rotor of high solidity. At high solidity there is a significant movement of mass flow form hub to tip and radial equilibrium does not exist. The variation of pressure from hub to tip of the rotor is typically about 10%.

Figures 15 and 16 show a comparison of predictions with experiments for pressure drop and efficiency respectively for a relatively larger diameter ($D_t = 0.6$ m) monoplane turbine.

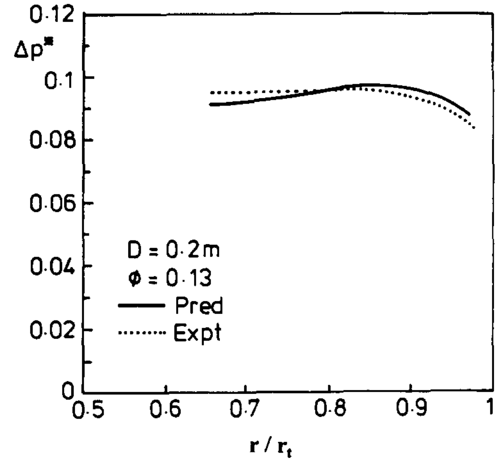

Fig. 13. A comparison of predictions with experiments for radial equilibrium of pressure.

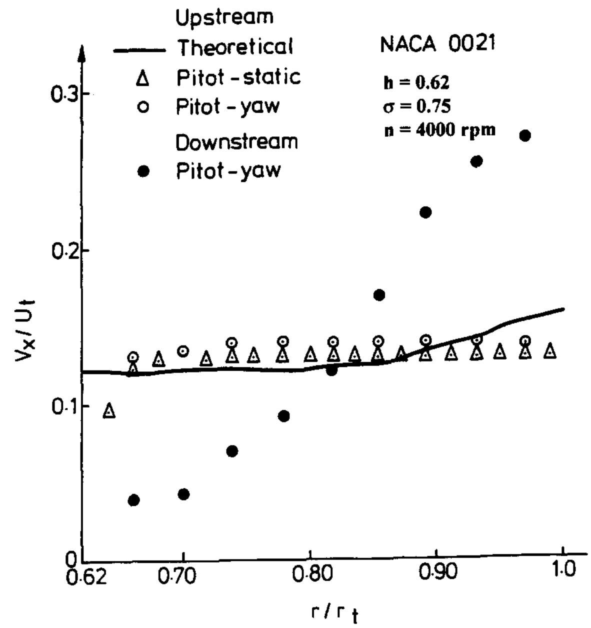

Fig. 14. Radial distribution of axial velocity at inlet and outlet of a Wells turbine: Predictions and experiments.

Figure 15 refers to the turbine without guide vanes and the Fig. 16 refers to the turbine with guide vanes. The prediction shown here is based on radial equilibrium theory and actuator disc theory. The agreement between predictions and experiments are generally good up to stall; differences at the stall are due to the uncertainty of predicting the stall for aerofoils in a cascade of 90° stagger. The pressure drop-flow rate characteristics (Fig. 15a) for this turbine are similar to those of the 0.2 m diameter turbine. The efficiencies (Fig. 15b) are higher than for the 0.2 m diameter turbine due to the larger scale (blade Reynolds number). There are no significant differences between the prediction methods and experiment for the pressure drops and the efficiencies. The actuator disc theory involves a correction to absolute airflow velocities based on radial equilibrium theory and for the Wells turbine these velocities are a small fraction of the relative airflow velocities and it appears that these corrections have only a small effect on the predicted values.

Predicted values of circulation in a non-dimensional form and at the exit of the rotor are compared with the data based on experiments in Fig. 15c. Although there are differences

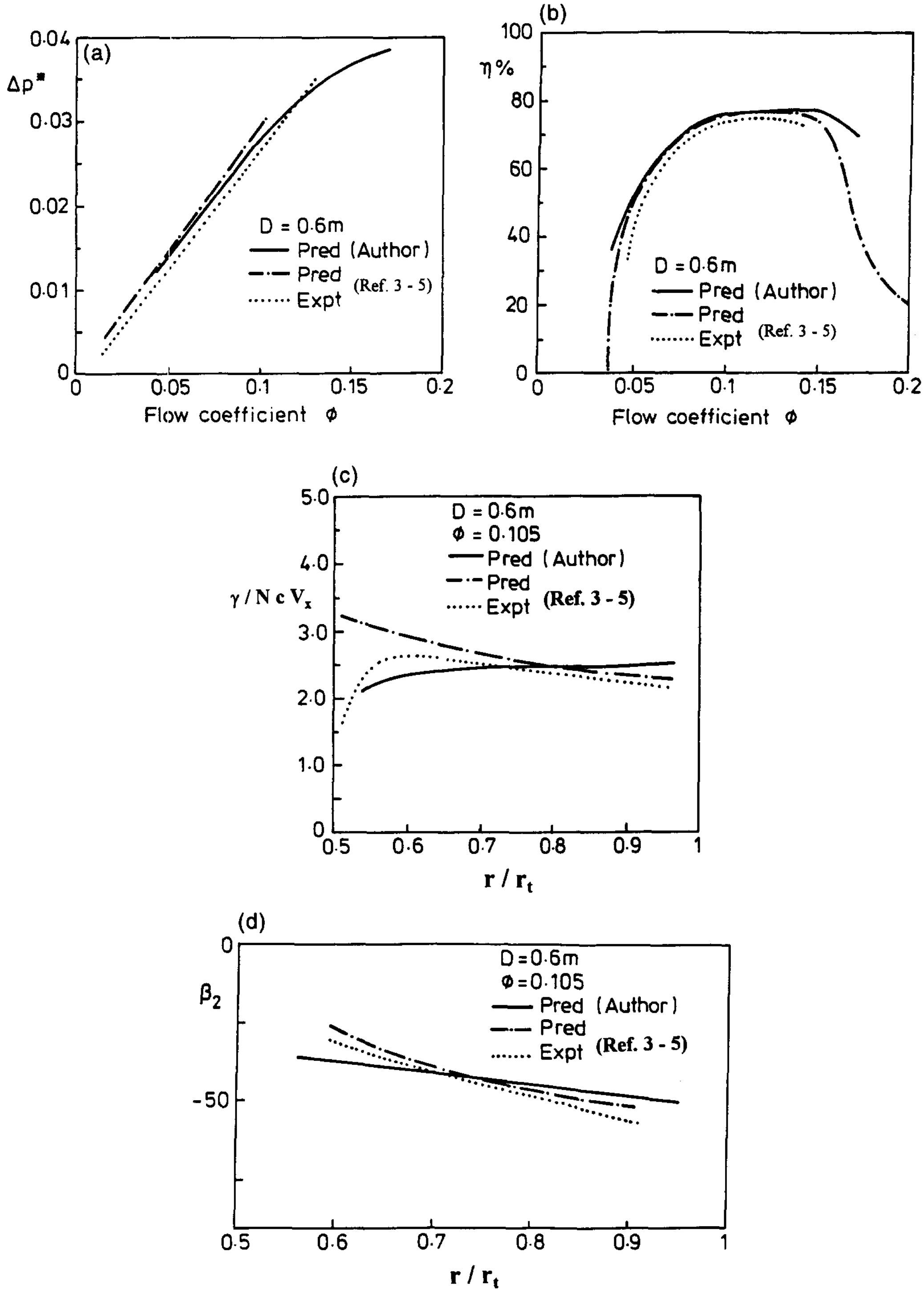

Fig. 15. A comparison of prediction with experiments for a 0.6 m diameter Wells turbine without guide vanes. (a) Pressure drop; (b) efficiency; (c) radial distribution of exit circulation; (d) radial distribution of absolute exit flow angles.

between prediction and experiments, this figure shows that the circulation at the rotor exit is virtually invariant with the radius except near the hub where it is likely that there is an effect on the circulation due to the boundary layer on the hub. The non-dimensional circulation γ^+ can be shown to be approximately proportional to C_l/α for a blade and for a linear

$C_l - \alpha$ relationship

$$\gamma^+ \propto \mathrm{d}C_l/\mathrm{d}\alpha$$

which indicates that the lift curve slope for the blades is approximately invariant with the radius. Further, the predictions for γ based on actuator disc theory compare more favourably with experiments than radial equilibrium theory. These results suggest that for a Wells turbine with a constant chord blade, the amount of work done by the blades is nearly the same at all radii and the exit flow is virtually free from vortex shedding.

A comparison of predicted and experimental values for the exit flow angle β_2 are shown in Fig. 15d. It is seen from this figure that the exit flow contains a significant amount of swirl ($\beta_2 \approx 40°$–$50°$). It can be shown by the prediction methods that the magnitude of swirl increases with the increase in solidity. A certain amount of swirl at the exit of the rotor may improve the overall aerodynamic efficiency by increasing the pressure recovery in the diffuser downstream of the rotor. Large levels of swirl at the exit would lead to high kinetic energy losses at the rotor exit which will result in a reduced overall efficiency.

The effect of introducing guide vanes[6] on the performance of the monoplane turbine can be observed from Fig. 16. The linear relationship between pressure drop and flow rate (Fig. 16a) is not altered by the introduction of guide vanes. The guide vanes produce slightly higher aerodynamic efficiencies (Fig. 16b) but leads to an earlier turbine stall. The reasons for this behaviour are discussed in Section 5.

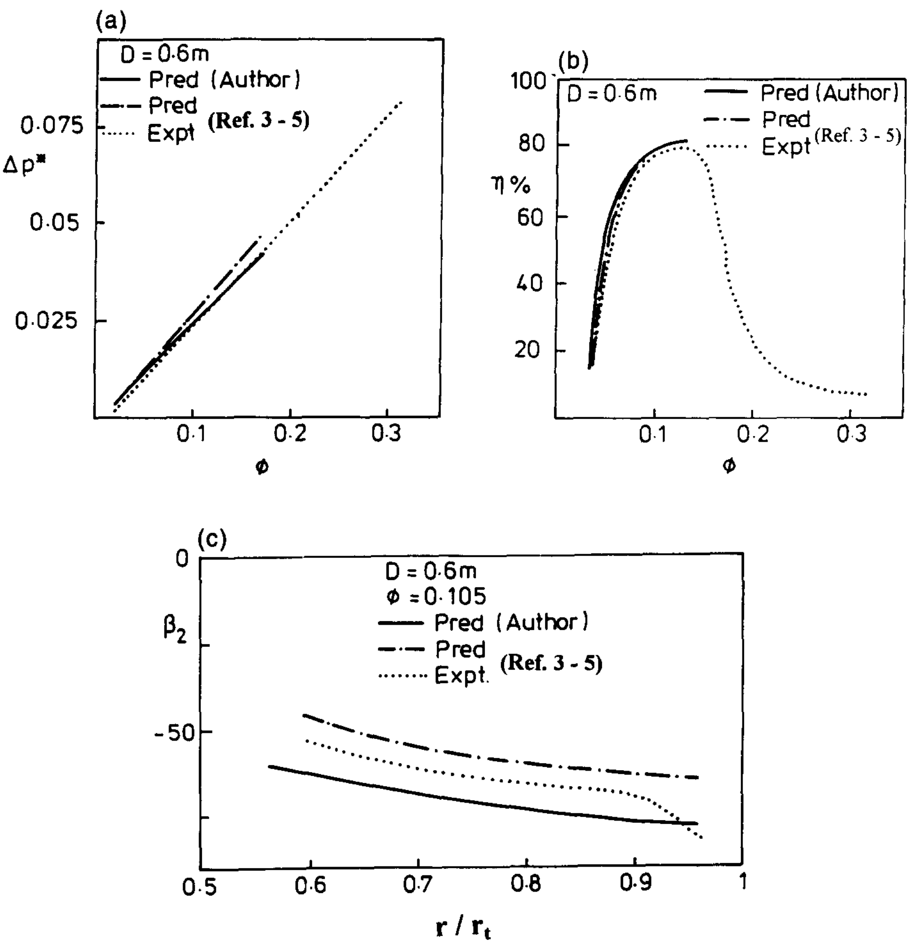

Fig. 16. The effect of introducing guide vanes for a monoplane Wells turbine: 0.6 m diameter. (a) Pressure drop; (b) efficiency; (c) radial distribution of absolute exit flow angles.

As regard to the exit flow angles (Fig. 16c) for the rotor with guide vanes discrepancies exist between the predictions and experiments. However this figure illustrates that the guide vanes result in a smaller swirl at the rotor exit. This swirl can be reduced even further by the exit guide vanes. For a Wells turbine in bidirectional airflow the inlet and exit guide vanes have to be a mirror image of each other.

4. PARAMETERS AFFECTING THE PERFORMANCE—MONO PLANE WELLS TURBINE

The aerodynamic performance of the Wells turbine is dependent on the aerodynamic force coefficients which in turn are a function of several parameters ϕ, σ, h, AR, ι, ι_e, T_u, f, M, and R to mention just some of them (Fig. 17). The performance is also affected by the generator characteristics.

The effect of flow coefficient on the Wells turbine performance has been discussed in Section 3. The effects of some of the other parameters on the performance of the Wells turbine are discussed in the following sections.

4.1. THE ROTOR SOLIDITY

The solidity of the turbine, σ, is a measure of blockage to airflow within the turbine. It is also a measure of the mutual interference between the blades and is an important design variable. Results based on the experimental data(11, 13, 14, 24, 26, 27, 37, 38, 51, 52, 54) for the average cyclic efficiency η normalised with respect to the corresponding two dimensional single aerofoil efficiency η_0 (Fig. 18) indicates that at small values of solidity the effect of solidity is small but significant reductions in efficiency occurs for $\sigma > 0.5$. The reduction in efficiency for a Wells turbine at high solidity is due to increased kinetic energy losses at the exit associated with the swirl. In addition there could be significant three dimensional effects near the hub where, at high solidity, the blades are close to each other and may interact with the boundary layer on the hub. These interactions may lead to boundary layer separation on the surface of the hub and also on the blade surfaces near the hub. These effects are compounded by the fact that the blades near the hub are always at a larger incidence that at the tip.

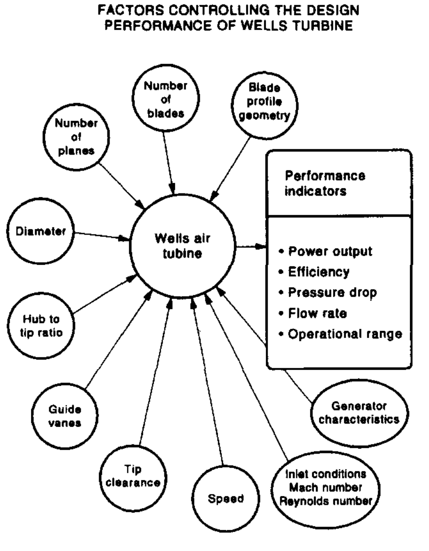

Fig. 17. Factors controlling the design and performance of the Wells turbine.

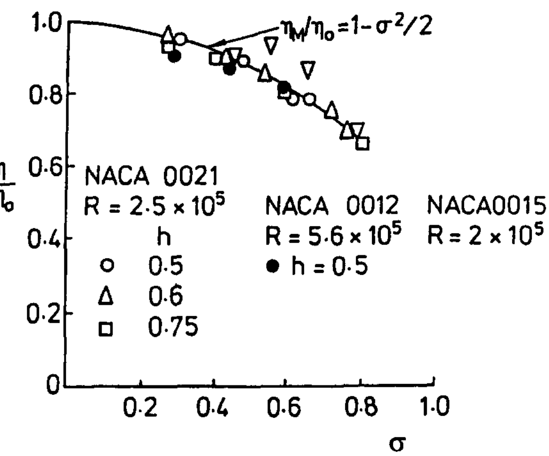

Fig. 18. Effect of solidity on efficiency: experimental data based on several references.

It was shown earlier that increase in σ also increases the pressure drop p^* (Fig. 6a). For a wave energy device with a large available pressure drop a high solidity turbine with a reduction in efficiency can be used. An alternative to this would be to use a biplane turbine; a two stage turbine without guide vanes. A low solidity turbine, however, does not have the ability to self start which is discussed in Section 6.

4.2. THE HUB-TO-TIP RATIO

The effect of hub-to-tip ratio h based on several works(4, 13, 26, 51) is shown in Fig. 19. Although the experimental data is taken from tests conducted at a fixed tip solidity of $\sigma_t = 0.4$, the aspect ratio, AR was not kept constant during the tests and therefore the results shown here have the combined effect of h and AR. The hub-to-tip ratio is an important parameter that for a fixed solidity and flow rate Q, the average axial airflow velocity V_x in the turbine annulus is a function of h given by

$$V_X = \frac{Q}{\pi D_t^2/4(1 - h^2)},$$

and the flow ratio at the tip ϕ_t is given by $\phi_t = V_X/U_t$.

The effect of hub-to-tip ratio on the turbine efficiency is rather complex. The hub-to-tip ratio has an effect on: (1) the airflow incidence at the hub (2); the leakage losses at the tip; and (3) the relative interference effects at the hub. For a turbine operating at a certain speed, the incidence at the hub is larger than the incidence at the tip and increases with a decrease in hub-to-tip ratio. Therefore it should be expected that a decrease in the hub-to-tip ratio should promote an earlier turbine stall and lead to a decrease in the aerodynamic efficiency. For a given tip clearance the hub-to-tip ratio determines the ratio of the tip clearance to blade height. A decrease in h reduces the ratio of tip clearance to blade height which should reduce the tip leakage losses and therefore improve the aerodynamic efficiency. On the other hand a decrease in the leakage of airflow around the tips produces a reduction in the so called relief effects (reduced spanwise flow near the tips) which can advance the stall on the blades. The aerodynamic efficiency is also subjected to the interference effects produced by the hub boundary layer. A decrease in h would reduce these interference effects and increase the efficiency. The results shown here, admittedly based on small-scale tests, suggest that the tip clearance and the hub interference have the dominating effect on the efficiency. Values of $h \approx 0.6$ are recommended for design.

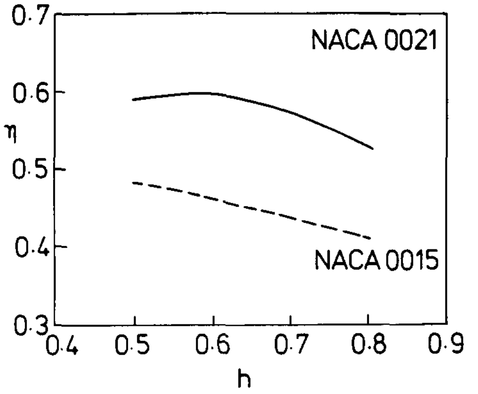

Fig. 19. Effect of hub-to-tip ratio on efficiency. $\sigma_t = 0.4$, — $R = 3 \times 10^5$, -- $R = 10^5$.

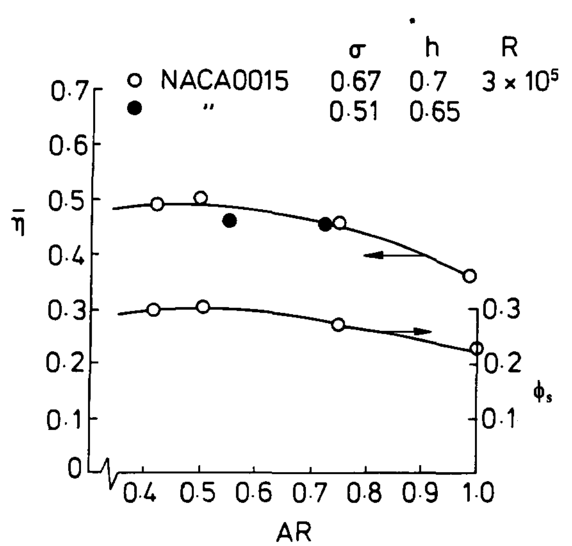

Fig. 20. The effect of aspect ratio on efficiency.

4.3. THE ASPECT RATIO

The aspect ratio, AR, influences the turbine efficiency and flow ratio at which the turbine stalls as seen from Fig. 20. The data shown here is from experiments conducted at a fixed hub-to-tip ratio and where the variation in the aspect ratio was obtained by varying the chord length. Therefore there is a certain influence of Reynolds number on this data. The primary effect of reducing the aspect ratio is to increase the efficiencies by postponement of stall, this is associated with the 'relief effect' obtained on the blades due to relatively increased mass flow through the tip. It has been observed(20,49,51) that the tip vortices become stronger as the aspect ratio is decreased. It has also been observed that the effect of aspect ratio becomes larger with the increase in tip clearance. AR = 0.5 could be a recommended value for turbine design.

4.4. THE TIP CLEARANCE

The Wells turbine is very sensitive to tip clearance t_c when compared to a conventional turbine. The effect of tip clearance on the turbine performance(13,41,55) is shown in Fig. 21. Decrease in tip clearance advances the stall but increases the cyclic efficiency as a result of reduced leakage losses. On the other hand a turbine with a relatively large tip clearance could operate over a much wider range of flow rate without stalling. In this respect there are no significant advantages to be obtained for $t_c > 0.02$. Therefore values of a tip clearance ratio $t_c < 0.02$ are recommended.

4.5. AEROFOIL THICKNESS RATIO

Figure 22 shows the effect of thickness ratio ι on the turbine efficiency.(13, 14, 29, 41, 51, 52) The effect of thickness ratio on the aerodynamic performance of aerofoil blades cannot be separated from the effect of the Reynolds number. The results shown in Fig. 22 are based on small-scale tests and therefore should be viewed with caution. These results indicate NACA aerofoil profiles of 20% thickness are most suited for the best performance. Thick aerofoil blades are also suitable for self starting characteristics of the turbine.

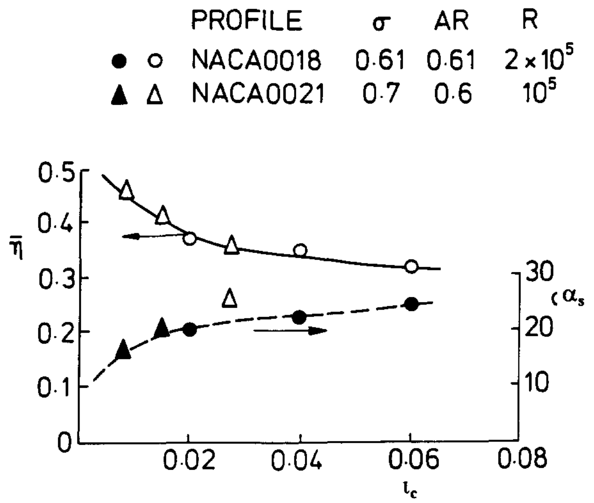

Fig. 21. Effect of tip clearance on efficiency and stall.

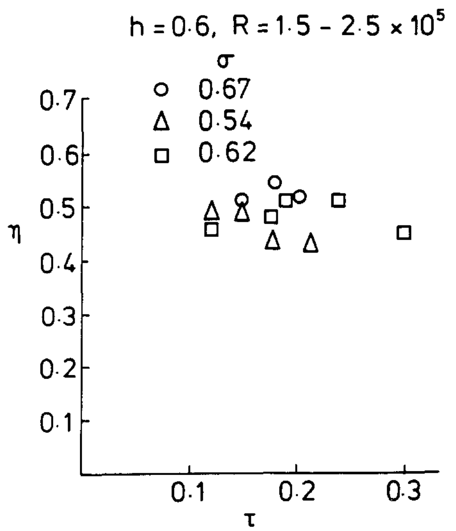

Fig. 22. Effect of profile thickness on efficiency.

4.6. THE BLADES OFF-SET

Most of the investigations on Wells turbine were conducted with rotors consisting of aerofoil blades of rectangular plan form. If it is assumed that the radial component of velocities in the rotor is negligible the velocity vector relative to the rotor would be in the circumferential plane and therefore normal to a radial line from the axis of rotation. For a blade of rectangular plan form, the leading or the trailing edge or both edges can be along lines which are not radial and this leads to sweep effects as illustrated in Fig. 23. If the leading edge of the blade is positioned along a radial line (Fig. 23a) it has no sweep but the trailing edge is subjected to a large sweep angle λ. At this condition the mid chord line of the blade is off-set at a ratio $g/c = 0.5$. The sweep angles at the leading and the trailing edges depend on this off-set and as g/c is decreased the sweep angles at the leading and trailing edges increase and decrease respectively (Figs 23a, 23b and 23c). For an a value of $g/c = 0$ both edges have equal values of λ (Fig. 23c). It should be noted that for a given g/c the sweep angles are also related to the blade aspect ratio. Flow visualisation on a rotor with blades of several planforms[52] (Fig. 23d) indicate a large effect of the blade sweep on the boundary layer separation on the blades. These results show that reducing the sweep angle at the leading edge of the blades reduce flow separation. One way to reduce sweep effects at the leading edge of blades of rectangular plan form is to reduce the off-set.[39] Figure 33 shows a large effect of g/c on both the aerodynamic efficiencies and the stall incidence for a Wells turbine. Although these findings are based on small-scale tests (low Reynolds number), where the boundary layer separation on the blades are sensitive to Reynolds number, it does point to the fact that sweep is an important factor in designing a Wells turbine. Based on the above results a value of $g/c = 0.15$ for the blades is recommended for the design.

4.7. THE INLET TURBULENCE

Turbomachines are sensitive to inlet flow conditions such as distortion of velocity profile and turbulence levels. Increase in turbulence levels can alter boundary-layer development by advancing transition of the boundary layer, and delaying stall. The performance of turbomachines can be improved by increasing the turbulence level at the inlet up to 3%.

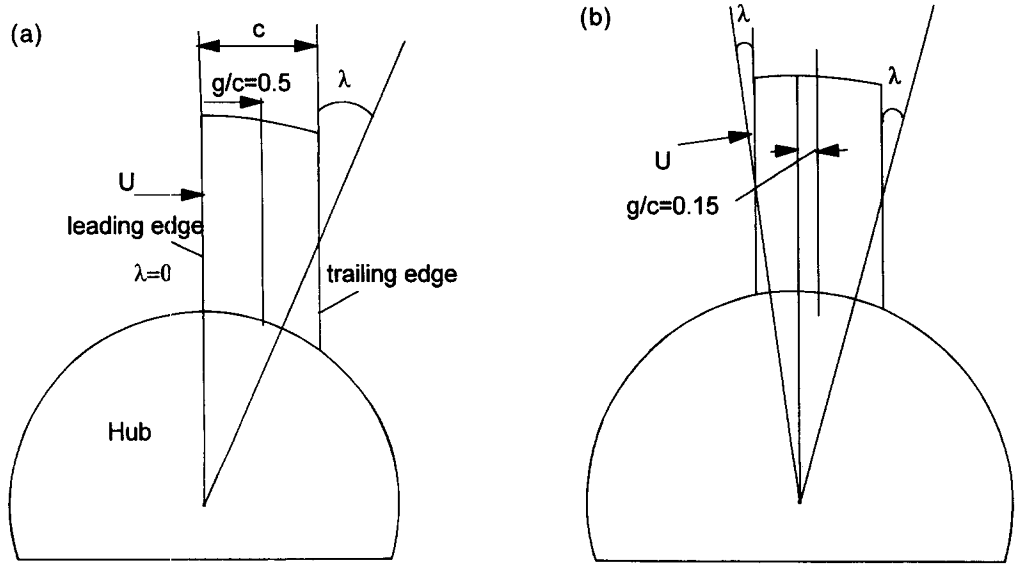

Fig. 23a, b.

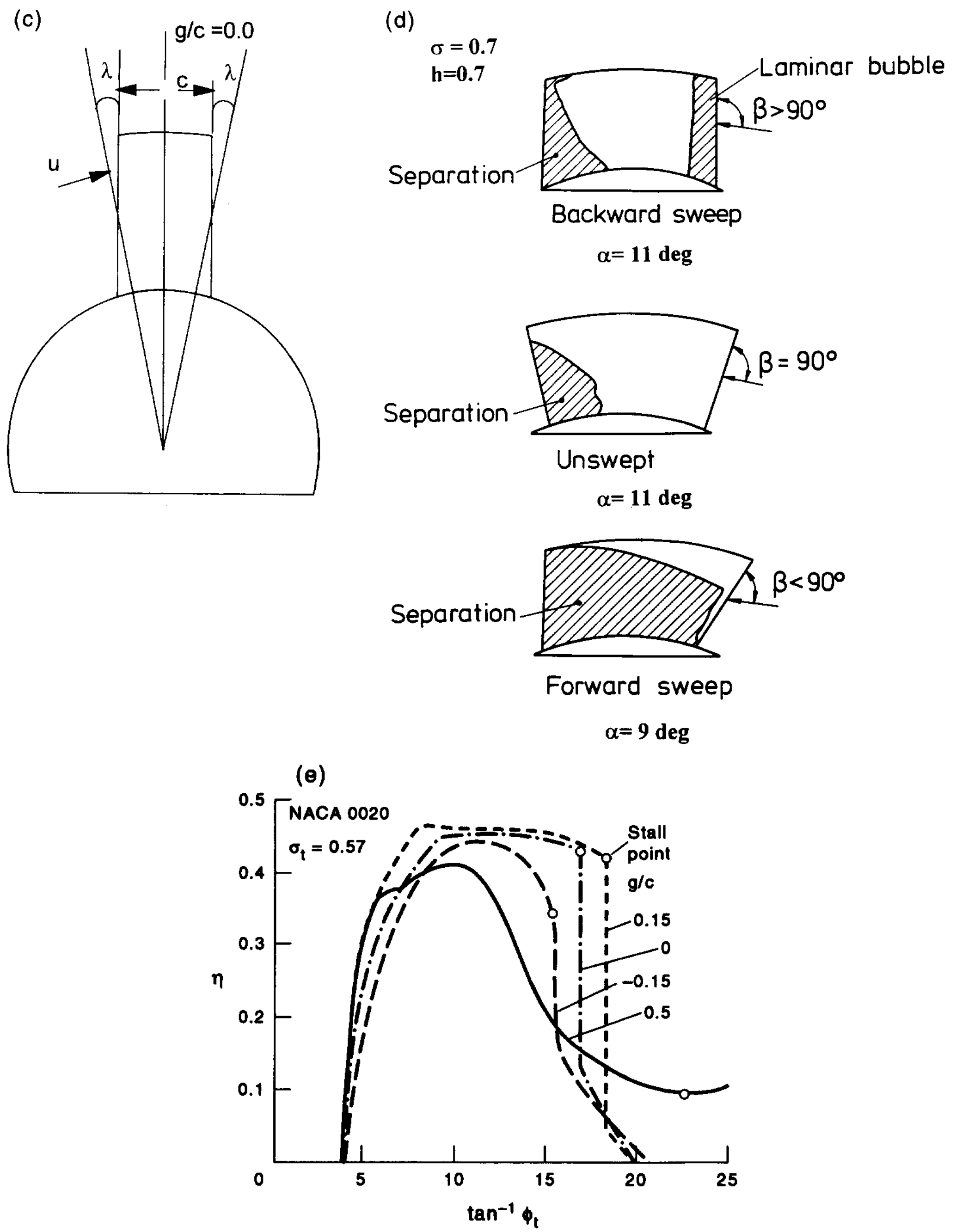

Fig. 23. The effect blade sweep on the performance of the Wells turbine. (a) The mid chord line offset by $g/c = 0.5$, leading edge has no sweep. Trailing edge has a large forward sweep angle. (b) The mid chord line offset by $g/c = 0.15$, the leading edge has a small backward sweep, trailing edge has larger forward sweep angle. (c) The mid chord line has no offset. The leading edge (backward) and trailing edge (forward) have equal sweep angles. (d) Flow visualisation on the Wells turbine blades with different sweep angles. (e) The effect of blade offset on efficiencies and stall.

Experimental results[33,38,41] (Fig. 24) indicates that the performance of the Wells turbine improves with an increase in turbulence but a significant increase in turbulence levels is required to produce any appreciable improvement in performance. It could be said that the Wells turbine is less sensitive to inlet turbulence compared to conventional turbomachines and this is due to the fact that absolute velocity at inlet relative to which turbulence levels are based is only a fraction of the rotor velocity.

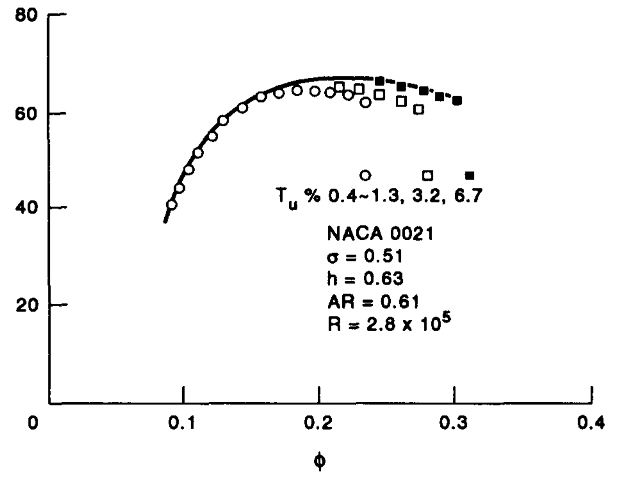

Fig. 24. The effect of free stream turbulence on aerodynamics efficiencies. The turbulence levels Tu are with respect to the relative velocity of the rotor.

4.8. THE EFFECT OF BI-DIRECTIONAL AIRFLOW

It is generally assumed that the airflow frequency in a wave energy device is so small (<1 Hz) that dynamic effects are negligible. All the results shown above are based on predictions based on quasi-steady assumptions or experiments conducted in uni-directional airflow test rigs. Calculated values of mean aerodynamic force coefficients on the blades, based on experiments on a Wells turbine in an oscillating airflow[17, 28, 34] are shown in Fig. 25a. It is clear from this figure that the turbine blades experience a hysteresis effect. The hysteresis effects are caused by asymmetry in the boundary-layer development on the blade surfaces and oscillating motion of the wake[34] the extent of which can be appreciable at low Reynolds numbers. The hysteresis effects also increase with the increase in the turbine solidity. These effects can be smaller on large-scale turbines where the boundary layer on the blades is essentially turbulent and relatively thinner. The effect of non-dimensional frequency f^* on cyclic efficiency[14, 28] (average efficiency over a cycle) on a small-scale

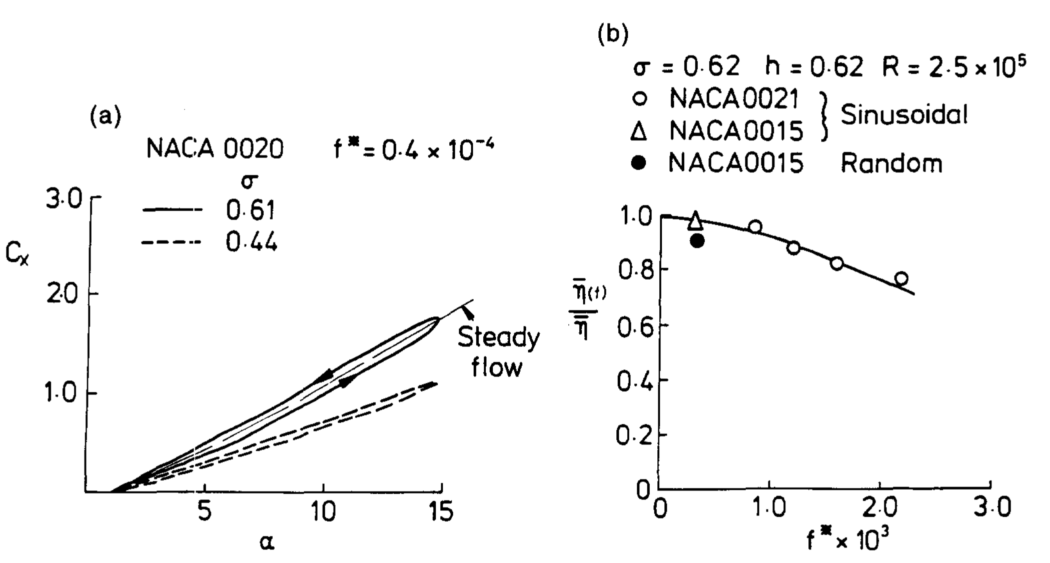

Fig. 25a, b.

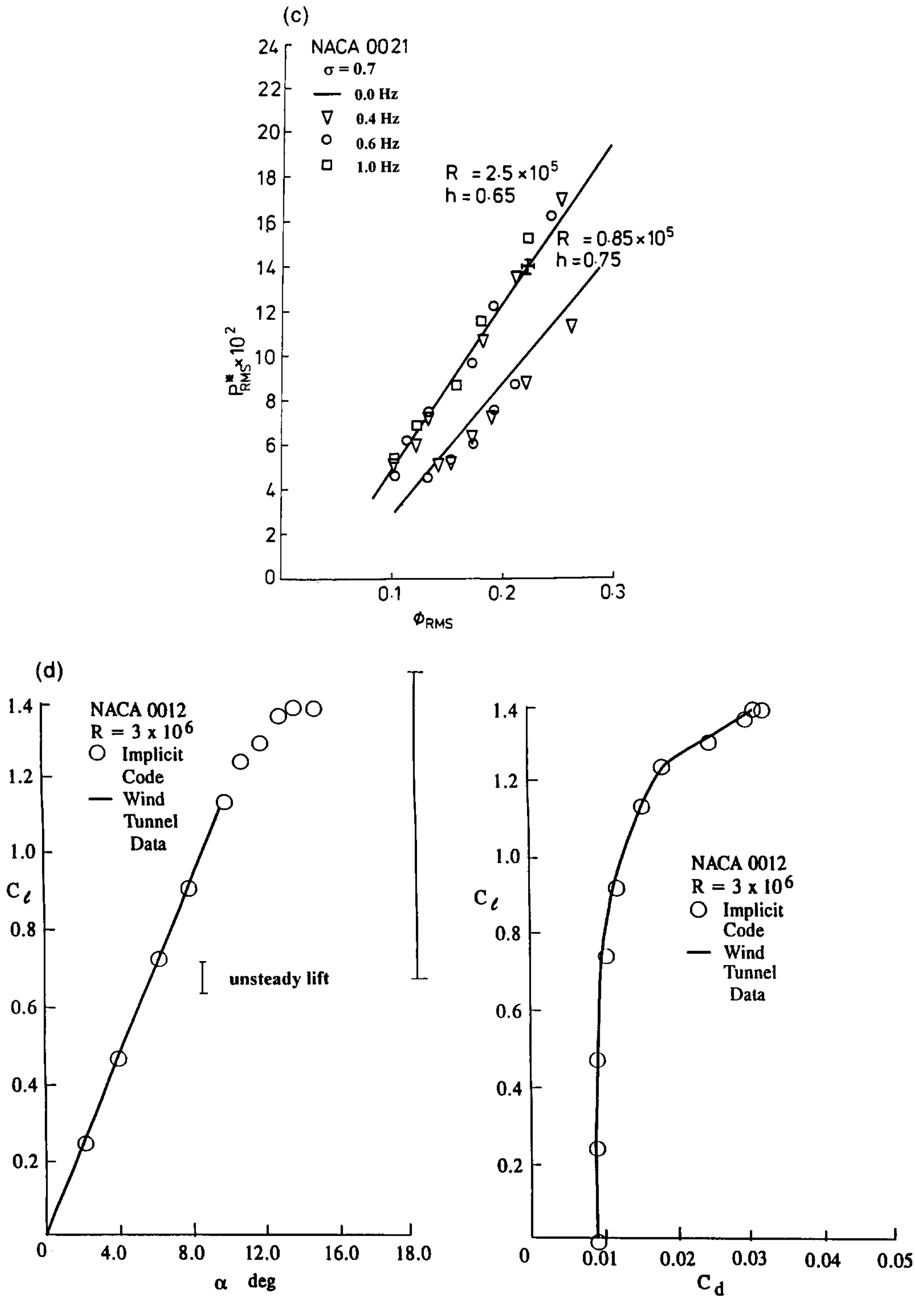

Fig. 25. The dynamic effects due to bidirectional airflow. (a) Hysterisis effects on axial force coefficients. (b) Effect of nondimensional frequency on efficiency. (c) Effect of frequency of airflow on pressure drop. (d) Dynamic lift forces on NACA 0012 aerofoil: predictions and experiments.

turbine can be observed from Fig. 25b. The normalised cyclic efficiency decreases with the increase in f^*. The performance of a turbine in sinusoidal flow is better than that in a random air flow where the turbine may experience small angles of incidence over long periods as discussed earlier. This is highlighted when the results from a device at sea are discussed in Section 5.2. In a sinusoidal airflow the effect of airflow frequency on the root mean square values of pressure drop is small (Fig. 25c).

Although a Wells turbine can be designed to operate within a certain range of $\pm\alpha$ where $\alpha \leq \alpha_s$, there would be instances of sea states when for a given speed the turbine will operate in a deep stall regime. Here the turbine blades will experience large unsteady forces as shown by the computed values of lift[44] for a range of incidence including stall for an isolated aerofoil (Fig. 25d). Under the conditions where the lift is unsteady the turbine blades will be subjected to buffeting which will reduce the life span of blades.

4.9. CRITICAL SPEED

The critical Mach number for an aerofoil is defined as the free stream Mach number for which the maximum local Mach number reaches unity. For free stream Mach numbers greater than the critical Mach number the flow over the aerofoil becomes transonic leading to shock wave formation and the associated transonic effects which can include significant increases in drag and buffeting. The former will result in reduction in aerodynamic efficiency and the latter reduced life of the blades. In the case of a Wells turbine the velocity which determines the critical Mach number is the relative velocity between the blades and the airflow which is primarily a function of rotational speed. Therefore if the transonic effects have to be avoided the Mach number based on the turbine tip speed has to be less than the critical. Computed values of critical speed for NACA0012 aerofoil in isolation and in a cascade of 90° stagger[57] are shown in Fig. 26. The calculations were based on the method of singularities in conjunction with the Prandtl–Glauert rule for the effect of Mach number. The figure shows that the critical Mach number is decreased considerably by the increase in solidity and increase in airflow incidence. It should be noted that the simple definition of critical Mach number given above leads to a pessimistic assessment of the adverse effects of the increasing incidence on the drag and buffet characteristics and so, Fig. 26 and the conclusions below present a very conservative picture.

Typically for a Mono plane Wells turbine operating at a solidity of 0.3 incidence range of $\pm 8°$, the tip Mach number has to be less than 0.4. The incidence and the Mach number at the hub are larger and smaller respectively, and it is important to ensure that the blades at

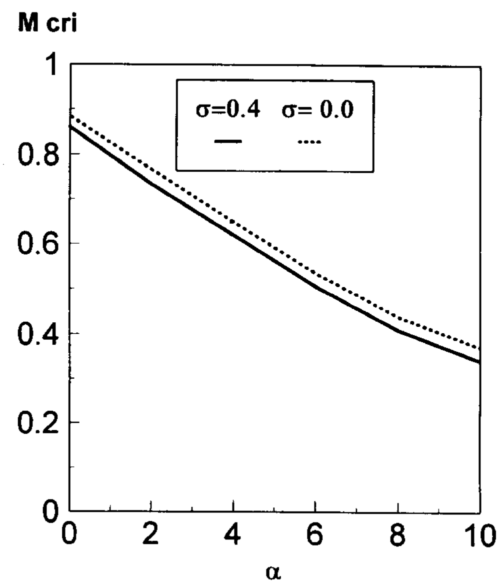

Fig. 26. Critical mach numbers for the Wells turbine blades with NACA 0012 profile, $\sigma = 0$ refers to a two dimensional aerofoil.

the hub are also operating at sub critical Mach number. It should also be borne in mind that the critical Mach numbers decrease with increase in aerofoil thickness ratio.

4.10. THE SCALE EFFECTS

The scale effect[31,41] on the turbine's maximum efficiency η_{max} is shown in Fig. 27. The figure includes experimental data from several turbine tests, predictions for a Wells turbine with NACA 0018 aerofoil blades (solid line) and predictions based on a scaling law for turbines in general[22] (dotted line) is given by

$$\frac{l-\eta_2}{l-\eta_1} = A + B\left(\frac{R_2}{R_1}\right)^{0.2}.$$

Here the experimental data is adjusted for a constant solidity of $\sigma_t = 0.67$ which will have self-starting characteristics for a Wells turbine (Section 8). It should be noted that the experimental results[4,6] are obtained from Wells turbine tests with guide vanes which affect the turbine's performance. The predictions are given for a turbine with NACA 0018 blades only because the data for NACA 0021 aerofoils over a wide range of Reynolds number are not available. When predicting using the scale law by the above equation, values of A and B are assumed to be 0.4 and 0.6, respectively, and the bench mark (η_1, R_1) for scaling was the QUB results with NACA 0021 aerofoil blades. It can be observed that there is a scatter in data at low Reynolds numbers. The discrepancy between the predictions and experimental data and the scatter of the experimental data to very low Reynolds numbers ($R < 10^5$) could be due to the following reasons. At low Reynolds number (small-scale) tests the friction in the bearings and windage losses form a significant part of the total power measured and the calculation of aerodynamic efficiency is subjected to considerable errors. The prediction method based on the above equation is based on the assumption that the boundary-layer on the blades is essentially turbulent which is unlikely at low Reynolds numbers. The predictions show that for a turbine with $\sigma_t = 0.67$, the maximum aerodynamic efficiency η_{max} for a large-scale Wells turbine ($R > 10^6$) can be typically 70% and much higher for a low solidity turbine (Fig. 18). As shown later the average efficiency of Wells turbine in random airflow encountered in a device at sea is typically about 60% (see Section 5).

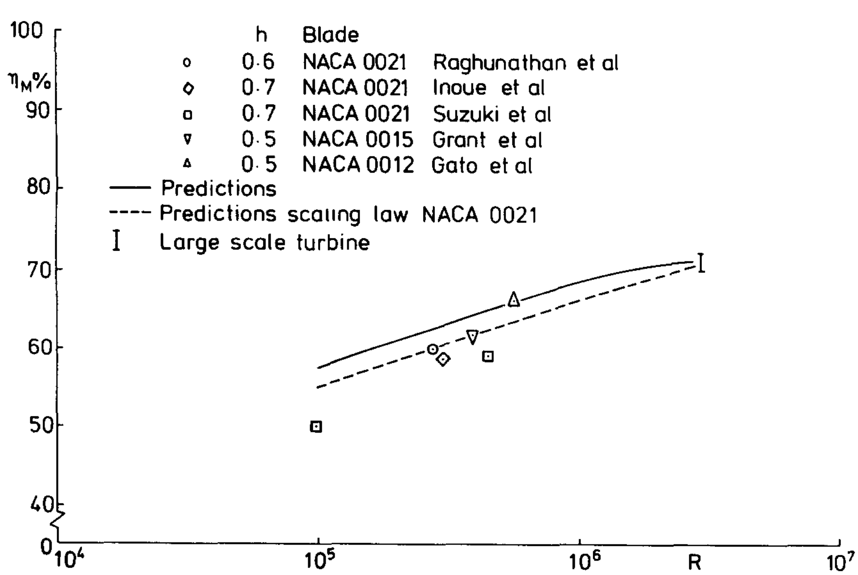

Fig. 27. Scale effects on the aerodynamic efficiency of high solidity, monoplane Wells turbine.

5. THE BI-PLANE WELLS TURBINE

The pressure drop across a single plane Wells turbine is proportional to the square of the tip speed which has to be limited if transonic effects are to be avoided. For wave energy devices which produce significantly larger pressure drops than the limit for a single plane turbine a multiplane(27, 32, 42) turbine (Fig. 4) can be used. Such a concept avoids the use of guide vanes and therefore the turbine would require less maintenance and repairs. The present state of knowledge on such a turbine is discussed below.

5.1. MUTUAL INTERFERENCE BETWEEN THE PLANES

In addition to the effects on the performance of a single plane rotor discussed above, the performance of a biplane rotor is subjected to additional aerodynamic interference effects between the planes of blades. These interferences are due to: (1) induced velocities by circulation on one plane on the other; (2) the wake produced by the blades in the upstream plane; and (3) the deflection of airflow produced by the upstream plane. These would effect both the lift (circulation) and drag produced on the blades.

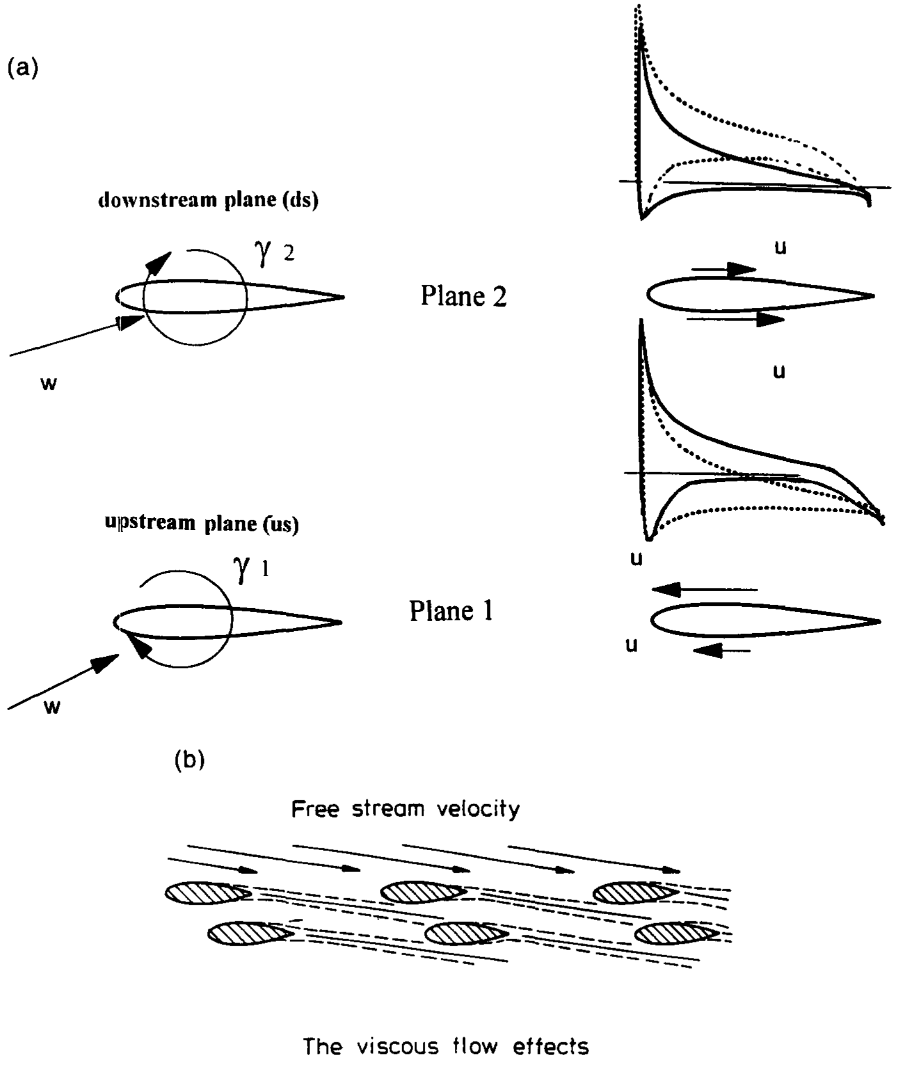

Fig. 28. Aerodynamics of a biplane cascade at a stagger angle of $\pi/2$. (a) Mutual aerodynamics interference between the planes due to bound vortices. The dotted line refers to pressure distribution due to induced velocities. The solid line refers to pressure distribution without interference effects. (b) Wake interference effects.

The mutual interference between the rows of blades exists in even inviscid flow due to the effect of the induced velocities of the blades in one plane onto the blades in the other plane as shown in Fig. 28a. The induced velocities (u) due to circulation on the upstream plane (γ_1) will lead to increased velocities on the surfaces of the blades in the downstream plane. But the increase in velocities on the upper surface of the blades should be smaller than that on the lower surface. Increase in the velocities and the corresponding decrease in pressures on the upper (suction) surface should lead to an advancement of stall and the relative increase in velocities on the lower (pressure) surface should lead to a decrease in lift for the blades in the downstream plane. The induced velocities due to circulation on the blades in the downstream plane (γ_2) lead to a decrease in the velocities on the surfaces of the blades in the upstream plane, with the decrease on the suction surface being greater than that on the

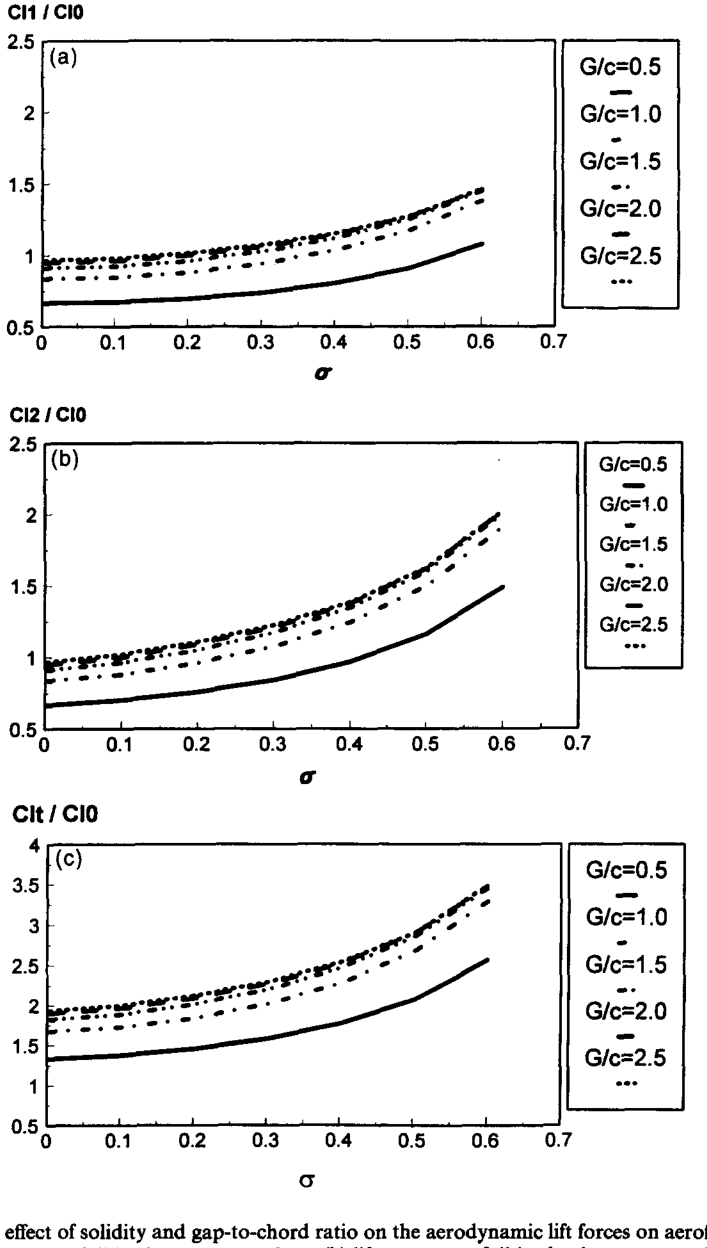

Fig. 29. Predicted effect of solidity and gap-to-chord ratio on the aerodynamic lift forces on aerofoils in a biplane cascade. (a) Lift on an aerofoil in the upstream plane; (b) lift on an aerofoil in the downstream plane; (c) total lift produced.

pressure surface. This should result in the postponement of stall and decrease of lift for the blades in the upstream plane.

The viscous effects are associated with the wake of the blades from the upstream rotor interfering with the flow on the blades in the downstream plane as shown in Fig. 28b. The deterioration of the performance of the downstream rotor due to this effect would be reflected by an increase in drag on the blades in that plane.

The magnitude of the above effects depends on the solidity in a plane, the gap to chord ratio between the planes (G/c) and the stagger between planes (Fig. 4). A simple model for evaluating the mutual aerodynamic interference effects between the blades in a biplane turbine is an infinite cascade of flat plates in a biplane configuration with vortex (Γ) located at 1/4c and the boundary condition that the normal component of velocity to the surface is zero at 3/4c for each of the flat plates.[48] Typical results based on this analysis for the variation in lift coefficient with solidity and gap to chord ratio, for an incidence angle of 10 degrees, and for plane 1 (upstream) and plane 2 (downstream) are shown in Fig. 29. The lift coefficients are normalised (C_l/C_{l0}) with respect to the corresponding value for an isolated flat plate. It can be observed from this figure that (1) for a given G/c, lift increases with σ as was the case for a mono plane cascade (Fig. 8d), (2) for a given G/c and σ, lift produced by the upstream plane (Fig. 29a) is smaller than that produced by the downstream plane (Fig. 29b), and (3) for a given σ, the mutual interference between the blades decrease very rapidly with the increase in G/c. For $G/c > 2$ the mutual interference between the planes are negligible. In fact small-scale experiments on a biplane Wells turbine has shown[27, 32] (Fig. 30) that the aerodynamic efficiency of the turbine is very nearly equal to that of a monoplane turbine if the gap between the planes is greater than the blades chord length. This means that for $G/c > 1$ a bi-plane rotor would behave like two monoplane turbines and each plane of blades can be analysed independently. In such a case the primary factor controlling the flow on the downstream rotor would be the deflection of airflow produced by the upstream rotor.

The effect of flow deflections on a biplane (without guide vanes) turbine performance can be seen from the airflow velocity triangles shown in Fig. 31a. It can be observed from this figure that for a biplane rotor without guide vanes the downstream rotor would experience smaller angles of incidence and larger relative velocities than the upstream rotor. The implications of these on the performance of a second rotor follow.

The aerodynamic efficiency of blades is proportional to the ratio of force coefficients C_θ/C_x and this ratio, for incidences less than stall angle, increases with incidence angle. For a given incidence for the upstream rotor the downstream rotor blades are at an incidence lower than that of the upstream and therefore will operate at a lower efficiency. For a given turbine speed the downstream should stall at a larger flow rate than that required for the

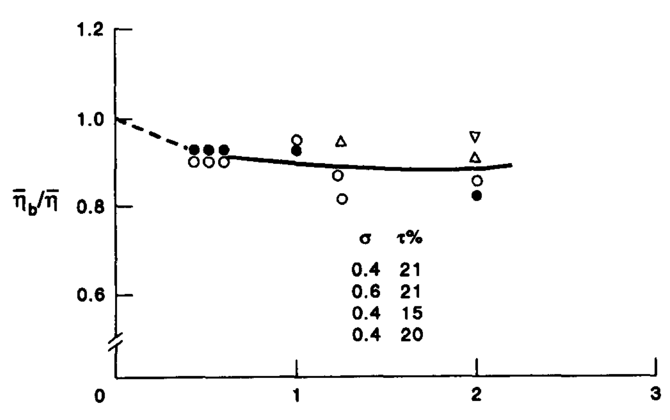

Fig. 30. Effect of chord-to-gap ratio on the aerodynamic efficiency of a biplane Wells turbine.

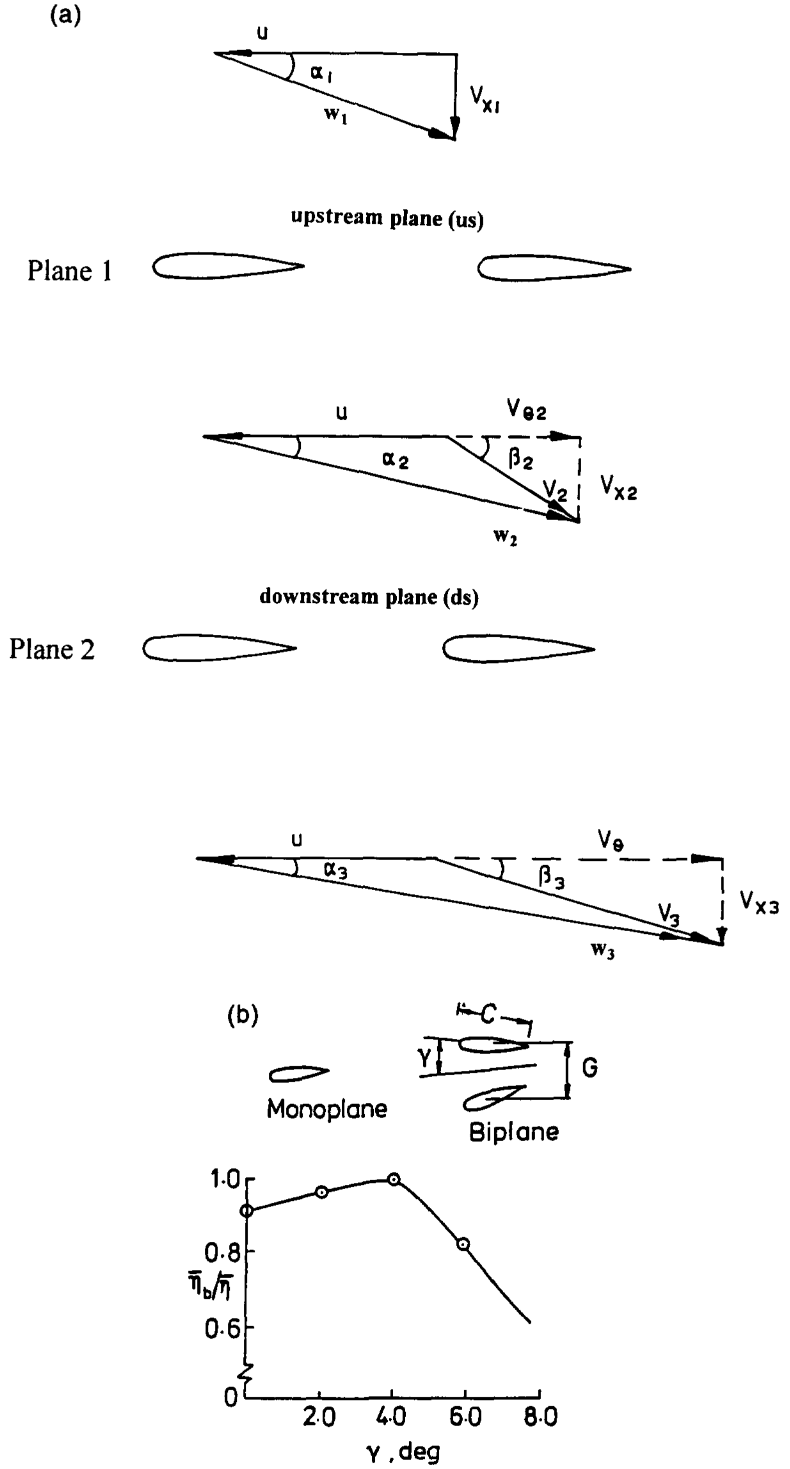

Fig. 31. The biplane Wells turbine without guide vanes. (a) The velocity triangles for a biplane without guide vanes; (b) the effect of pre-set incidence to the blades.

upstream rotor. Further, the kinetic energy losses due to swirl at the exit of a biplane rotor is considerably larger than that at the exit of a monoplane rotor which is detrimental to the overall efficiency of the turbine. Since it is the airflow velocity relative to the rotor which limits the turbine speed (to avoid transonic effects) the speed limit for a biplane turbine is controlled by the maximum relative velocity of the downstream rotor. This would mean that for a given flow rate a biplane turbine has to operate at a lower speed than that of a monoplane turbine. The effective airflow incidence to the upstream rotor can be reduced and correspondingly the airflow incidence to the downstream rotor increased by pre-setting the blades at an incidence to the plane of rotation.[18] Such a configuration can increase the turbine efficiency as shown in Fig. 31b.

The effects on flow velocities of introducing guide vanes for a biplane rotor designed for certain maximum flow rate and the same turbine tip speed are illustrated in Fig. 31a. The velocity triangles shown here are for a rotor with symmetrical inlet and outlet guide vanes with absolute velocities between the planes axial. With guide vanes designed in this way the downstream rotor (plane 2) would behave like a monoplane rotor with the swirl taken out by the outlet guide vanes and therefore would have relatively high aerodynamic efficiency. In addition to this the inlet guide vanes would produce relatively greater flow incidence to the upstream rotor (plane 1). This has the effect of increasing the aerodynamic efficiency but advancing the stall on the blades in that plane. The reduced relative velocities will produce a relatively lower pressure drop and therefore lead to a mismatch between the turbine and the device. A solution to these problems would be to operate the turbine at relatively larger speeds to compensate for the above effects. Figure 32b illustrates the effect of increase in turbine speed of a rotor with guide vanes to a level where the relative velocity of airflow is the same as that for a biplane rotor without guide vanes. It can be observed from Fig. 32 that a biplane Wells turbine running at a relatively larger speed can operate at the same stall angle and produce the same pressure drop as that of a biplane turbine without guide vanes. It also has the advantage of reduced kinetic energy losses at the exit.

5.2. THE PERFORMANCE OF A BIPLANE WELLS TURBINE

Although there are some experimental data available from the Islay biplane Wells turbine tests there are no data available for a medium- or large-scale turbine under controlled conditions. The understanding of the performance of biplane Wells turbine described in the following sections are primarily based on small-scale experiments, available data from the Islay turbine and predictions.[42] In predicting the performance of a biplane Wells turbine it is assumed that the gap-to-chord ratio between the planes is sufficiently large that the primary factor controlling the performance of the downstream plane is the deflection of air produced by the upstream plane. It is assumed that the radial equilibrium for pressure exists for both planes and the blade elements stalls at an incidence of 15°.

The results of the prediction for pressure drop p^* and efficiency η are compared for a small-scale biplane Wells turbine in Fig. 33. The comparison shown here is for a Wells turbine 0.2 m in diameter running at 5000 rpm. The turbine had 4 blades, (NACA 0021 profile) in each row and at a solidity of 0.5 per plane. The pressure drop shown (Fig. 33a) is the average pressure drop per plane and the efficiency (Fig. 33b) is the total rotor aerodynamic efficiency. It is observed from these figures that the agreement between prediction and experiments is good considering errors involved in small-scale measurements.

The Islay Wells turbine has the following specifications: tip diameter $D_t = 1.2$ m, hub-to-tip ratio $h = 0.62$, blade profile NACA 0012, blade chord $c = 0.4$ m, number of blades per plane $N = 4$, speed $n = 1500$ rpm, Gap to chord ratio $G/c \cong 1.0$. Predictions for this turbine are given in Figs 34 and 35. Predictions are compared with the Islay tests in Fig. 36.

Figure 34a shows the variation of efficiency η with flow rate ϕ for planes 1 and 2. It is observed that plane 1 produces a much higher peak efficiency (80%) but stalls earlier when compared with the results of plane 2 which has a peak efficiency of 60%, consistent with earlier discussions on biplane turbine without guide vanes. The variation of non-dimensional pressure drop p^* with ϕ for the two planes are shown in Fig. 34b. The $p^* - \phi$ relationships are linear for both the planes but plane 2 produces about a 50% higher pressure drop than plane 1. This is due to the occurrence of larger relative velocities and Mach numbers for the blades in plane 2.

The variations with radius of circulation γ normalised with respect to the value at the turbine mean radius are shown in Fig. 34c. The variation of circulation with radius at the

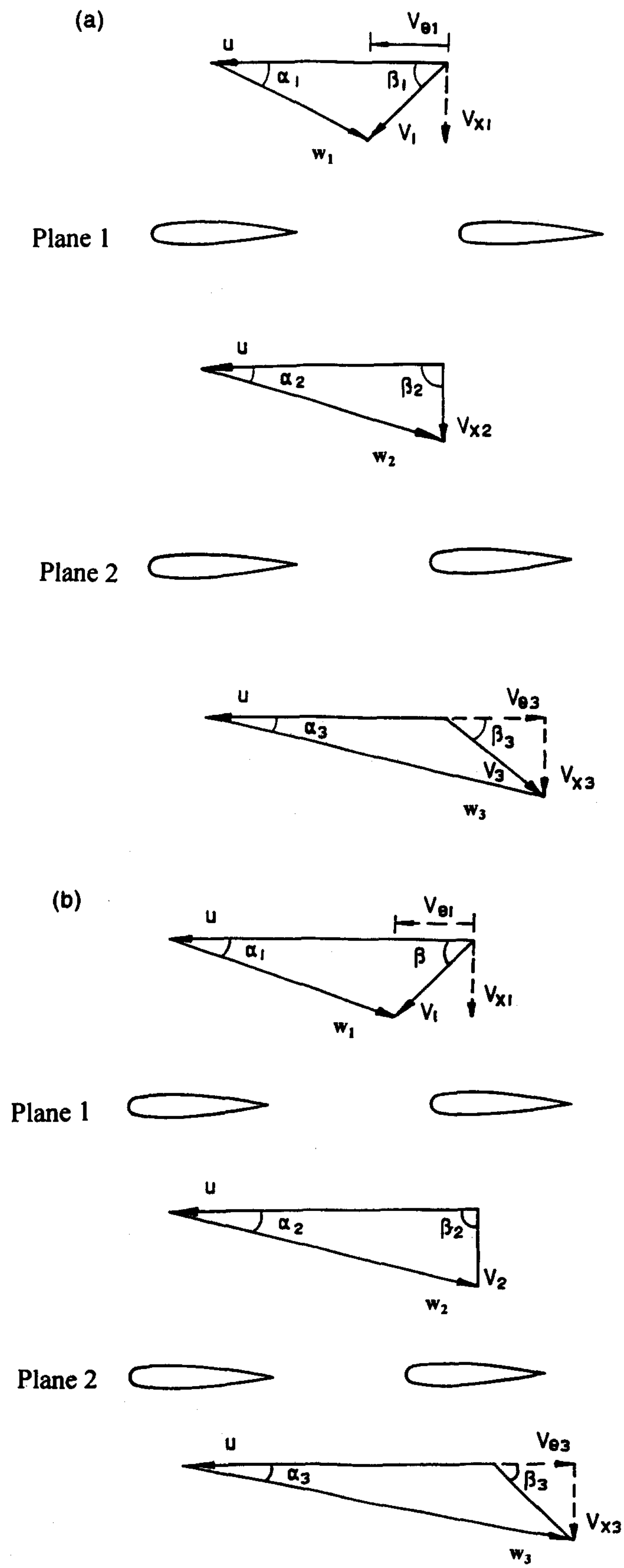

Fig. 32. The biplane turbine with guide vanes. (a) Velocity triangles for a biplane turbine with guide vanes; (b) the effect of increase in speed for a biplane turbine with guide vanes.

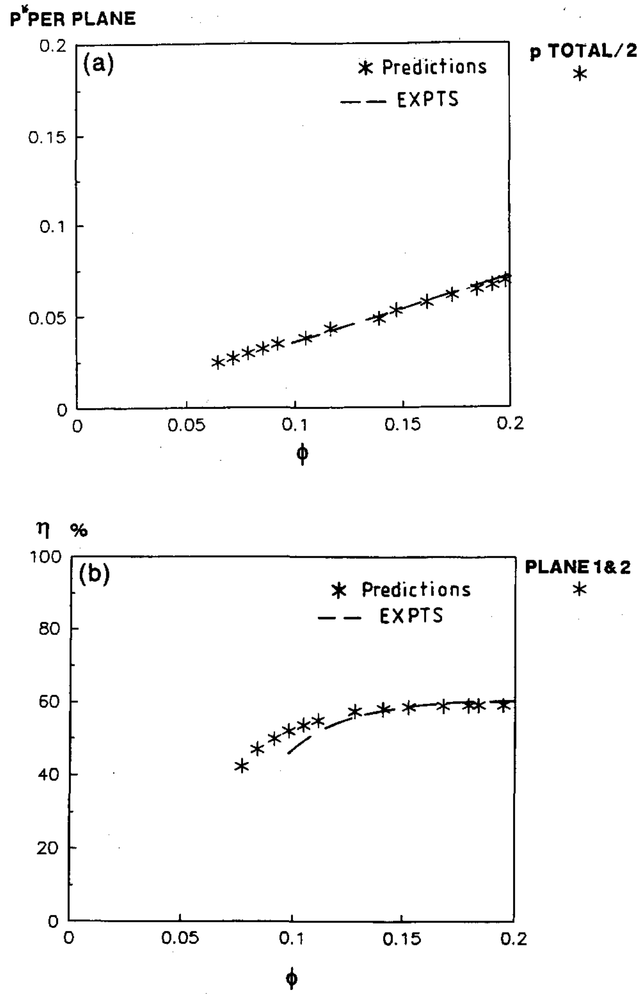

Fig. 33. A comparison of predictions with experiments for small scale biplane turbine $D_t = 0.2$ m. (a) Pressure drop; (b) efficiency.

exit of plane 1 is small, within $\pm 5\%$, indicating that the vortex shedding of the blades is negligible and the work done is virtually invariant with the radius for the blades in plane 1. The variation of γ with radius for plane 2 is somewhat larger ($\pm 15\%$) and therefore the blades in plane 2 do produce a certain amount of vortex shedding which may be detrimental to the overall efficiency of the turbine. Figure 34d shows the variation of non-dimensional total energy drop P_o^* with radius for the two planes. The variation of P_o^* with radius is negligible for plane 1 which is not the case for plane 2 where it appears that more work is done at the tip than at the hub. The variations of kinetic energy of airflow KE* with radius normalised with respect to the pressure drop (Δp) for the two planes are shown in Fig. 34e. The kinetic energy of the airflow at the exit of plane 2 is approximately 35% of the pressure drop across that plane. The kinetic energy losses due to swirl are larger at the hub than at the tip. Without the guide vanes this exit kinetic energy loss represents an appreciable part of the overall energy losses in the turbine. The significant amount of swirl produced can also be inferred from Fig. 34f which shows the variation of exit flow angle with radius for planes 1 and 3. The flow appears to leave the second plane at small angles of between 15 and 20° to the plane of rotation.

The effect of adding guide vanes to the same turbine as above but running at a higher speed of 2000 rpm (due to reasons given earlier) is shown in Fig. 35. At a speed of 2000 rpm the rotor with the guide vanes produced approximately same average flow rate and pressure drop as the rotor running at 1500 rpm without guide vanes. In predicting the performance

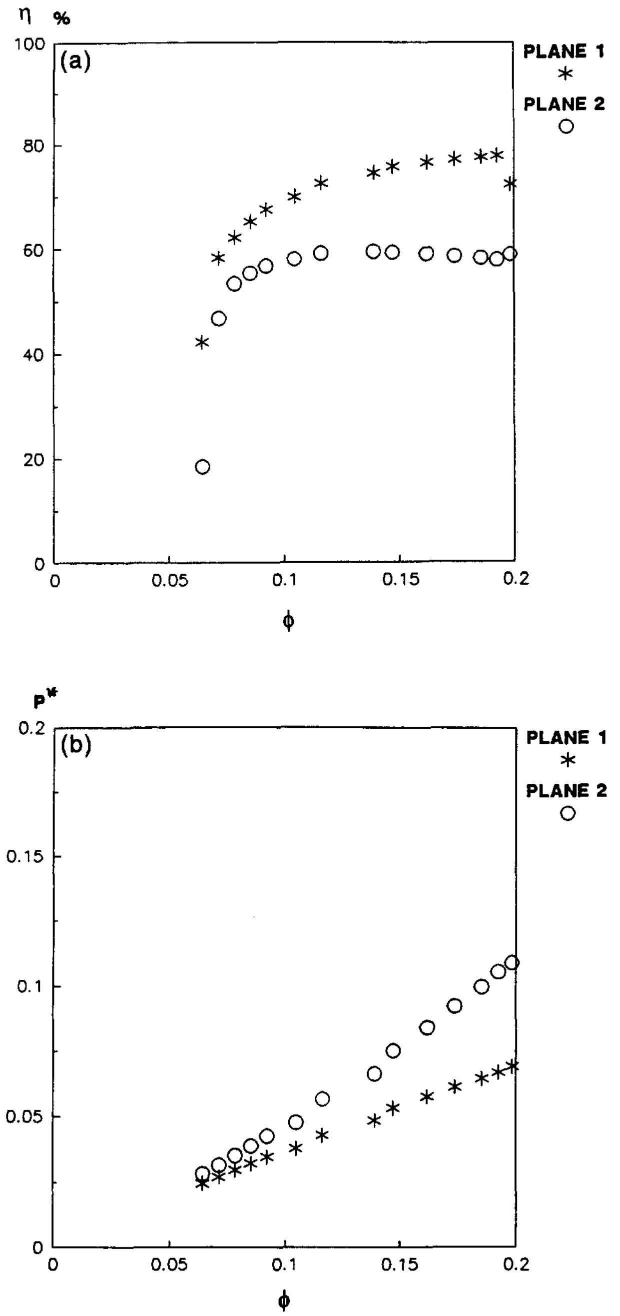

Fig. 34a, b.

of the rotor with guide vanes, the angle of the guide vane at the inlet β_1 was set at 35° at the hub and variation of β_1 with radius was such that the inlet flow was swirl free. Figure 35a shows that guide vanes can significantly improve the efficiency of a biplane turbine. The reasons for this improvement have been discussed earlier. With the guide vanes plane 1 appears to stall at a relatively lower value of $\phi = 0.11$. But it should be noted that the turbine is rotating at a higher speed and the flow rate at which the stall occurs is the same for both turbines, with and without guide vanes. The linear pressure drop-flow rate behaviour of the turbine is preserved with guide vanes as seen from Fig. 35b. Plane 2 still produces a larger pressure drop when compared to plane 1. The values of p^* appear to be lower than that of the biplane without guide vanes because of the relatively higher speed of

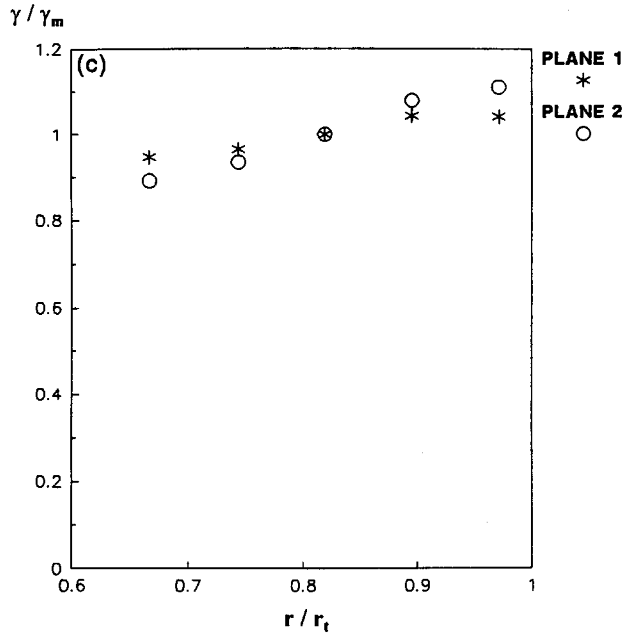

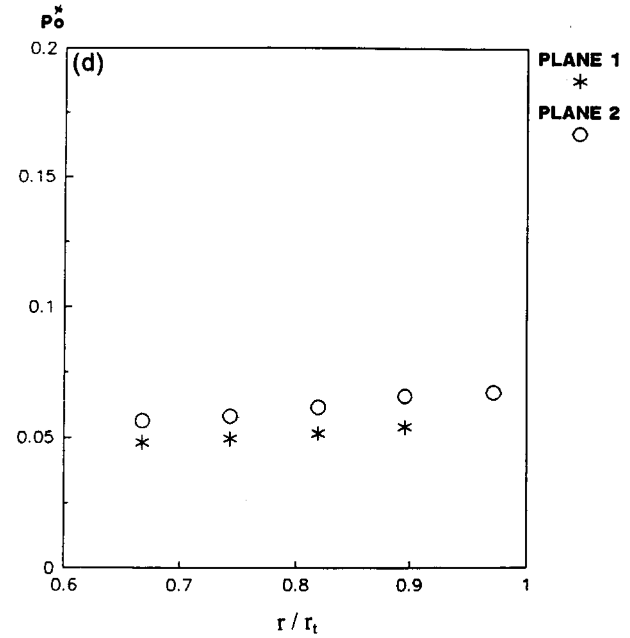

Fig. 34c, d.

operation. As mentioned earlier the speeds chosen are such that the turbine with and without guide vanes produces the same average pressure drop.

The overall energy drop P_0^* is the same for both plane 1 and plane 2 as can be seen from Fig. 35d. The result of the introduction of guide vanes is also to produce relatively lower kinetic energy losses (KE*) at the exit of rotor 2 (Fig. 35e). As a fraction of the pressure drop the kinetic energy of flow is only 15% compared to 35% for a biplane turbine without guide vanes. A part of this kinetic energy can be recovered by the exit guide vanes. The flow angles with radius at the entry to the inlet guide vanes (β_1), exit of plane 1 (β_2) and entry to exit guide vanes (β_3) for the biplane rotor with guide vanes are shown in Fig. 35f. The inlet guide vane angle was set at 35° at hub and varies with radius. For a Wells turbine the exit guide

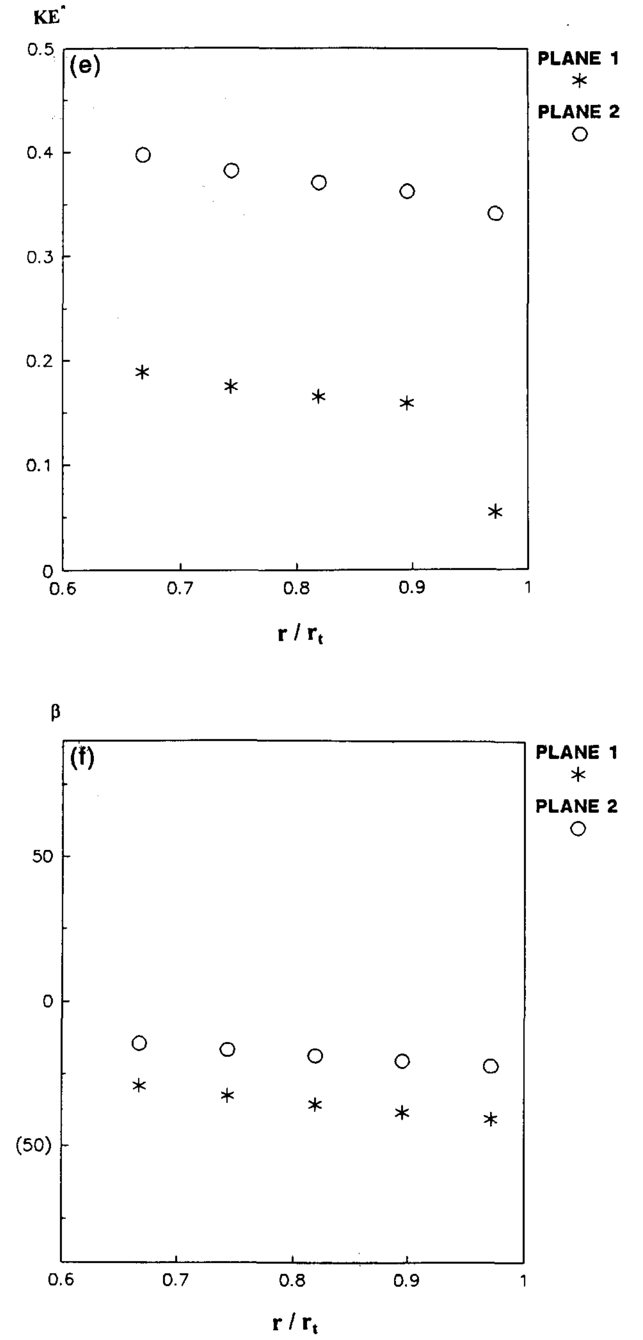

Fig. 34. Prediction of the performance of a medium scale bi-plane Wells turbine without guide vanes $D_t = 1.2$ m. $n = 1500$ rpm. (a) Efficiency; (b) pressure drop; (c) radial distribution of circulation at exit planes $\phi = 0.14$; (d) radial distribution of total pressure drop at exit planes $\phi = 0.14$; (e) radial distribution of kinetic energy at exit planes $\phi = 0.14$; (f) Radial distribution of flow angles at exit planes $\phi = 0.14$.

vanes have to be a mirror image of the inlet guide vanes. The figure shows that this is only approximately fulfilled for the conditions chosen. The exit and inlet guide vane angles are within 15° of each other. It should be mentioned that setting guide vanes with larger deflections of airflow at the inlet and outlet may lead to large guide vane losses. In order to minimise the guide vane losses a symmetrical guide vane system can be designed with smaller deflections at the inlet and outlet with intermediate guide vanes set between plane 1 and plane 2.

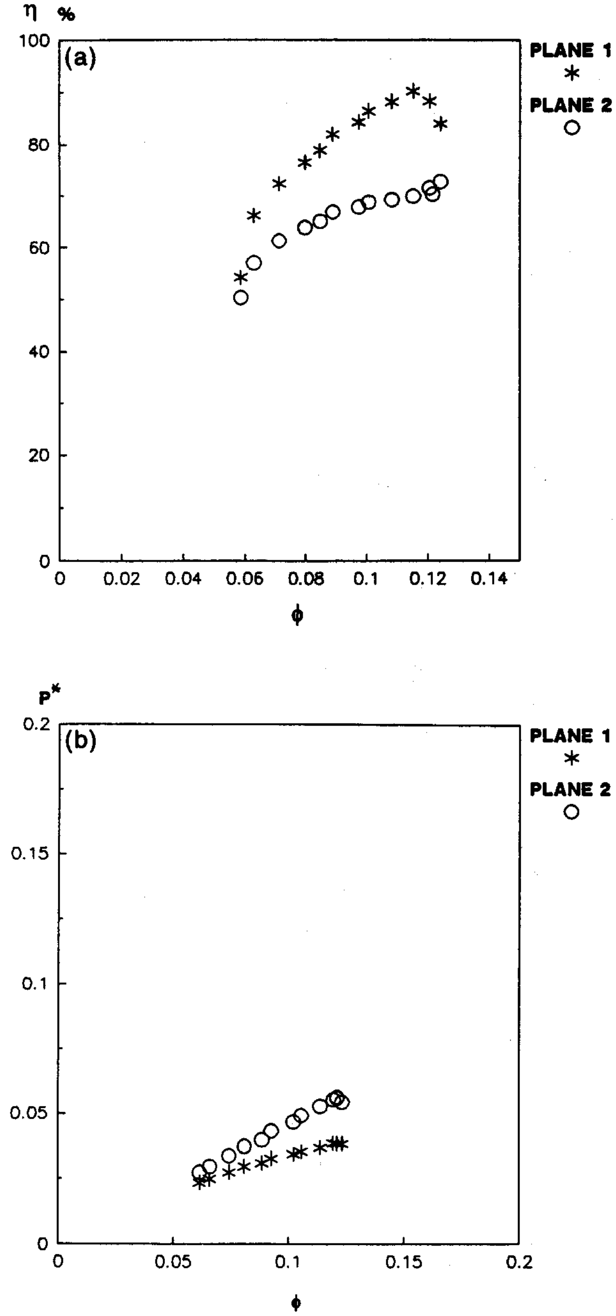

Fig. 35a, b.

A comparison of predictions based on the quasi-steady assumptions with experimental data from the device at Islay in Scotland is shown in Fig. 36. Details of this turbine generator section[43,59] is shown in Fig. 1. In this device one would expect the airflow velocities to vary randomly with time. Details of the experiments and the analysis techniques are given in Ref. 59. The predictions here are for inlet velocities sampled at 0.2 s intervals. Although the trend of predicted values with time for the pressure drop (Fig. 36a), efficiency, (Fig. 36b), and power output (Fig. 36c) agree favourably with the experimental results there are some significant differences. The predicted values underestimate the pressure drops and overestimate the efficiencies and power output. There are many reasons for these discrepancies. These include the inadequate modelling of the onset of boundary

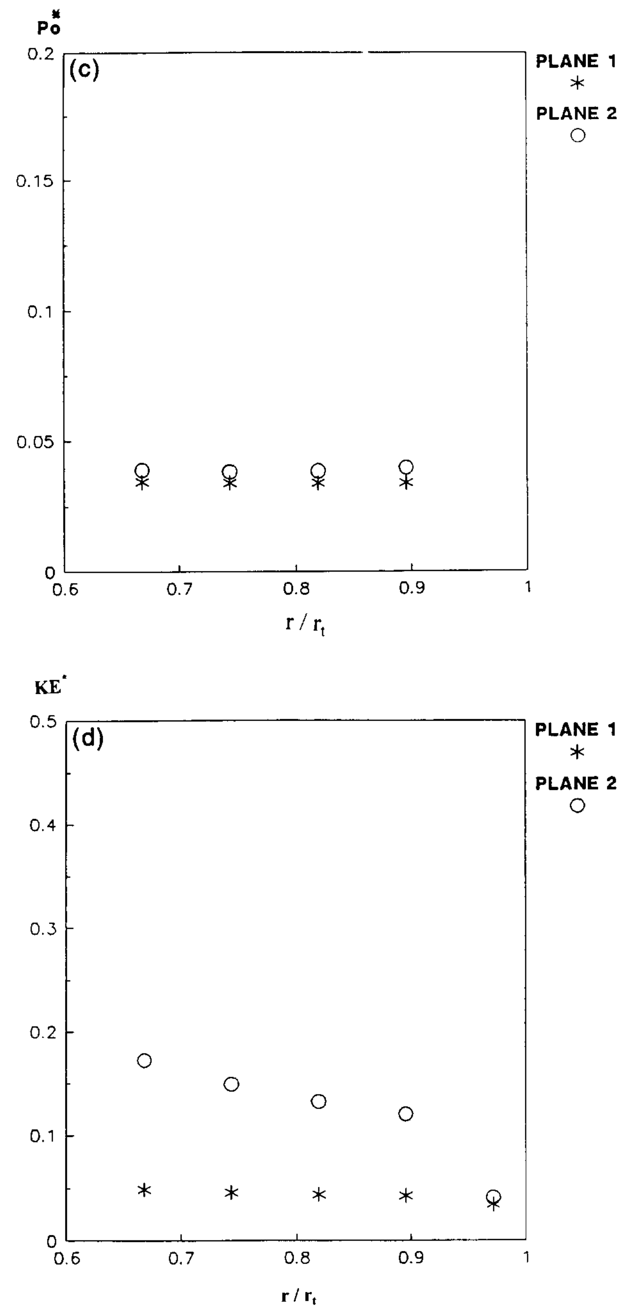

Fig. 35c, d.

layer separation on the blades and behaviour of flow once it is separated, three dimensional boundary layer effects and errors associated with measurements in a bidirectional and random airflows to mention some of them. Further to these, the flow at the entry to the turbine was measured to be far from uniform due to inadequate entry length for the turbine (Fig. 1). The flow distortion at the inlet was also caused by the butterfly valve in the inlet duct. Therefore the predictions could be regarded as only first order accurate.

6. THE STARTING PERFORMANCE OF A WELLS TURBINE

In a wave energy system an important design consideration is the self starting capabilities of the turbine. The phenomenon encountered with the Wells turbine, where the turbine

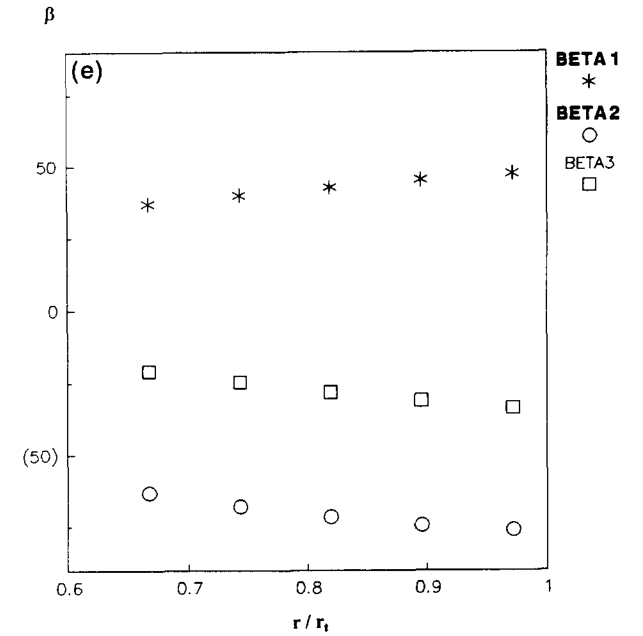

Fig. 35. Prediction of the performance of a medium scale bi-plane Wells turbine with guide vanes. $D_t = 1.2$ m, $n = 2000$ rpm, β_1 (hub) $= 35°$. (a) Efficiency; (b) pressure drop; (c) radial distribution of total pressure drop across planes $\phi = 0.11$; (d) radial distribution of kinetic energy at exit planes. $\phi = 0.11$; (e) radial distribution of flow angles at inlet and exit planes. $\phi = 0.11$.

accelerates up to a certain speed which is much lower than the running speed for the best performance, can be termed crawling[24] and this can be explained by the observation of a typical variation of tangential force coefficient C_θ with incidence α for a symmetrical aerofoil[35, 36] for an incidence range $\alpha = 0$–$90°$ as shown in Fig. 37a. Four distinct regimes for C_θ are noticeable. When the turbine starts from rest, the value of α is 90°. At this incidence C_θ is positive and the turbine starts rotating. If it is assumed that the axial velocity at the inlet is constant with radius, then, the incidence angle should decrease as the rotor speed increases. The value of C_θ is positive in regime IV enabling the rotor to keep on rotating. The operating regime for the turbine is about a point A close to the stall angle in the regime II and in order to move into regime II, the rotor has to pass through regime III where the force coefficients are negative. The inability of the rotor to pass through III results in the crawling phenomenon. The mean aerodynamic torque coefficient calculated from turbine tests[12,17,24,25,52] in a unidirectional flow are shown in Fig. 37b. It is observed from this figure that crawling can be virtually eliminated at high rotor solidity where regime III becomes insignificant. The reduction in the negative region with an increase in solidity has also been confirmed by cascade tests.[35]

The hub-to-tip ratio also plays an important part in the ability of the turbine to avoid crawling. As mentioned earlier for a given turbine speed, the incidence at the hub is relatively larger than that at the tip. The relative difference of the incidence angles increases with the decrease in the hub-to-tip ratio. Therefore it is conceivable that during the starting of the turbine rest the blade sections near the hub could be in a regime say IV generating a positive torque while the blade sections near the tip are in the regime III with negative torque and the blades could be generating a net positive torque. The effects of hub-to-tip ratio h and solidity σ_t on the ability to run up to operational speed are shown in Fig. 37c. The closed symbols indicate conditions for self starting. It is clear that low values of h and high values of σ are needed for self starting. The simulation studies on the Wells turbine[12] also confirm these findings. Figure 37d shows the variation of speed ω normalised with

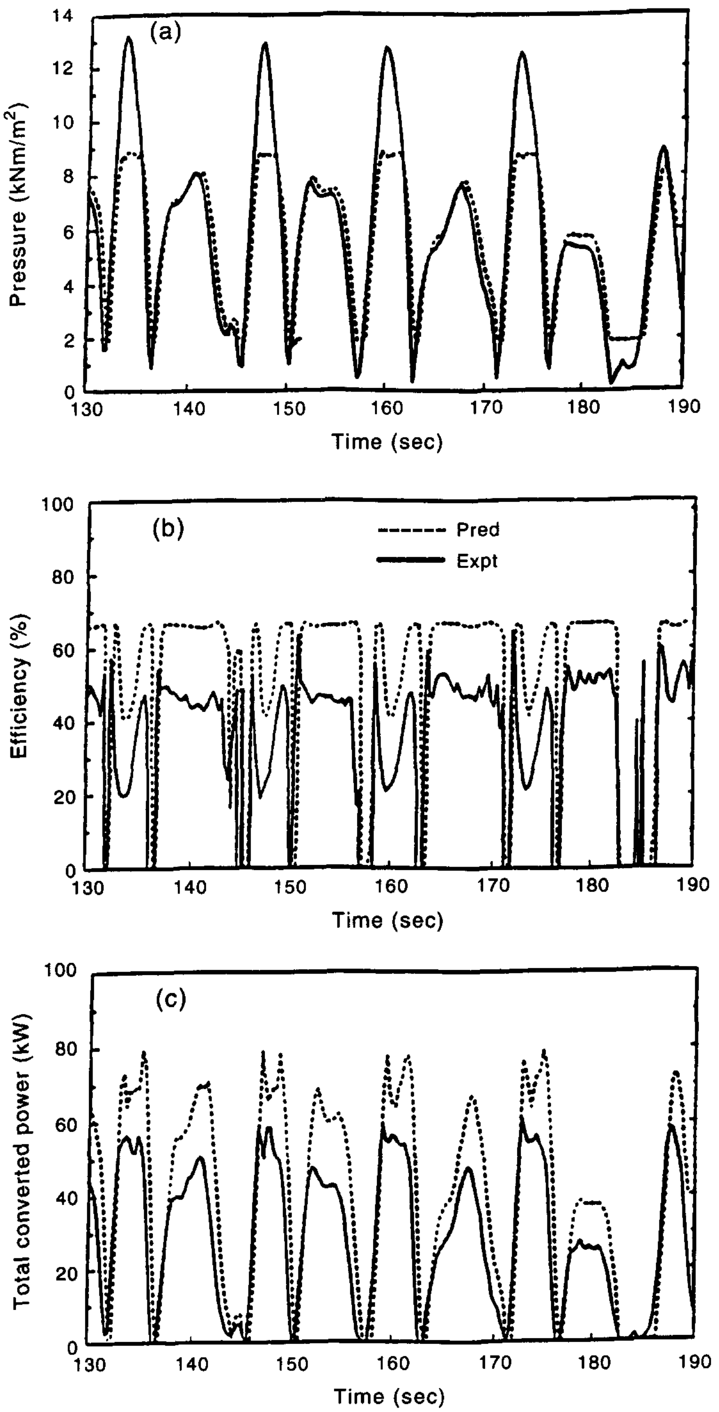

Fig. 36. A comparison of prediction with measurements: Islay bi-plane Wells turbine. $D_t = 1.2$ m, $n = 1500$ rpm (no guide vanes). (a) Variation of instantaneous pressure drop with time; (b) variation of instantaneous efficiencies with time; (c) variation of power output with time.

respect to operational speed[41] as a function of the number of cycles from starting for a turbine in an oscillating airflow. It can be observed that for a high solidity of $\sigma = 0.67$ the turbine runs up to full speed within 20 cycles. The turbine with $\sigma = 0.57$ has only a crawling speed which is only a fraction of the required operational speed.

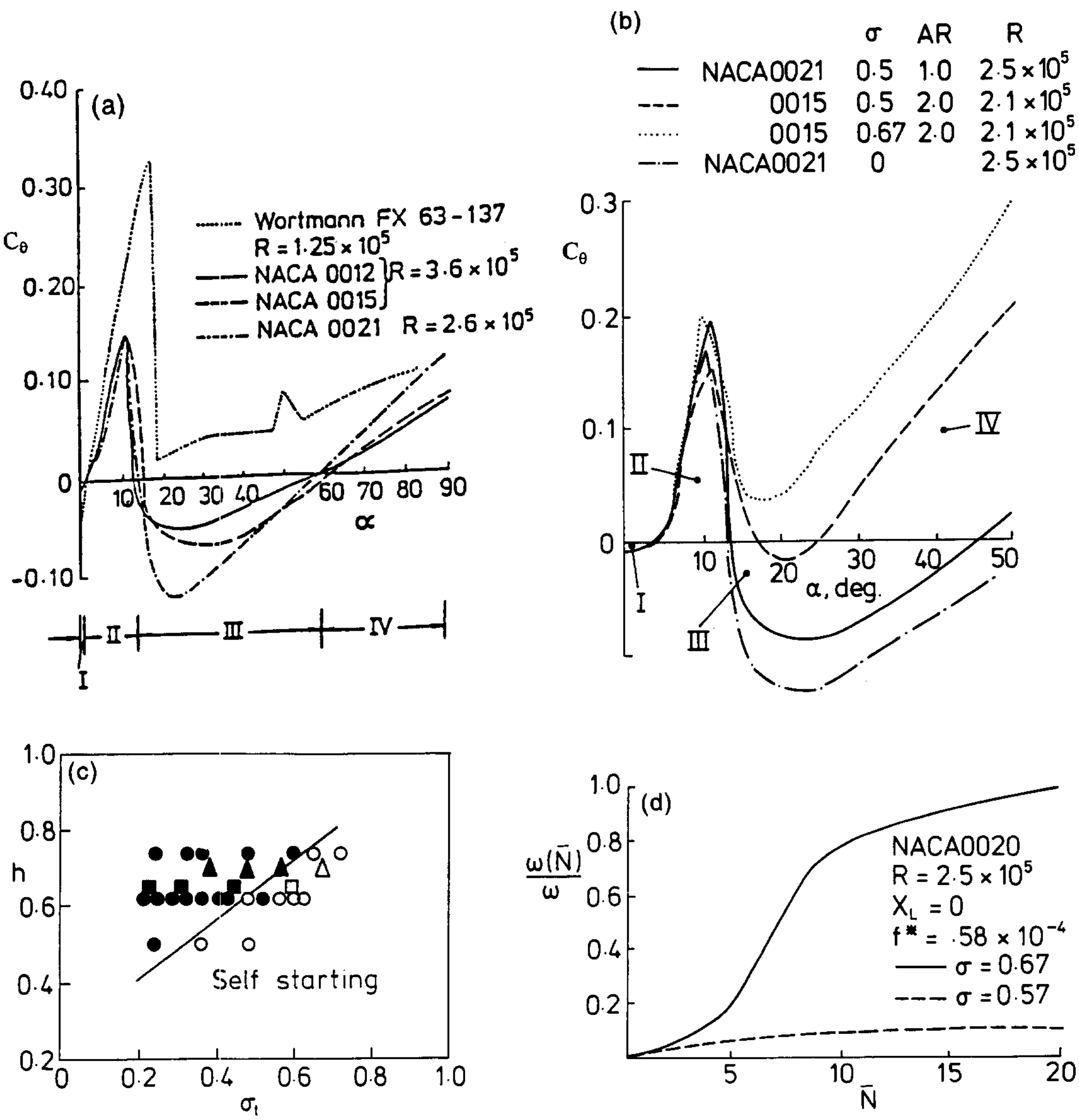

Fig. 37. The starting performance of a monoplane Wells turbine. (a) Effect of incidence angle on the peripheral force coefficient for $0 < \alpha < 90°$; (b) regions for peripheral force coefficients; (c) the relative effects of hub-to-tip ratio and solidity on the ability of the turbine to self start: (d) ability of the turbine to run up to operational speed in a bi-directional airflow.

7. SOME CONCEPTS TO IMPROVE THE PERFORMANCE OF WELLS TURBINE

The Wells turbine, although well suited to energy conversion of the wave energy devices based on the principle of an oscillating water column, has inherent limitations in its performance range with regard to flow rate. For a given turbine speed, at low flow rates (small incidences) the turbine absorbs power whereas the maximum flow rate is limited by the onset of stall. In a wave energy device at sea the flow rates do vary over a very wide range such that the turbine may be operating at either small incidence angles or very large incidences over significant periods. The former leads to a considerable reduction in the overall time-averaged efficiency while the latter would mean that the device would not be able to convert all the power available from the wave motion and also, the life span of the blades would be reduced. In the absence of guide vanes the exit kinetic losses could be considerable particularly for a turbine of high solidity. The turbine can experience hub stall and has tip speed limitations. There could be several ways by which these problems can be alleviated. These include: (1) variable speed; (2) variable blade incidence by having a movable flap[39] or variable pitch (movable blades);[5,47,50] (3) movable guide vanes; (4) by-pass;[47] (5) contra-rotating rotors;[1,45] (6) active or passive control of boundary layer on the blades;[44] (7) boundary layer control on the hub and (8) blade sweep.

The variable speed turbo generator can be designed either as a variable speed device within a cycle with the mean speed varying from cycle to cycle depending on the wave amplitudes or as a variable speed machine where the speed is fixed for a group of waves of similar amplitude and speed varying from one group to another.

The movable flap arrangement could consist of a trailing or leading edge flap whose incidence is varied within a cycle with the extent of variation depending on the amplitude of waves. The advantage of a flap can be observed from results of small-scale experiments[39] in a uni-directional airflow where a series of tests were made with fixed flap angles (Fig. 38). The primary effect of a leading edge flap is to increase the operating range for flow rates with a small reduction in the peak efficiency. At small flap angles (5°) the trailing edge of the flap is very close to the leading edge of the blade with negligible mass flow in the gap between the flap and the blade. The effective geometry is not a streamlined shape and the flap has a detrimental effect on the turbine efficiency. The flap is effective for a flap angle of typically 20 degrees. Similar beneficial effects can be achieved with trailing edge flaps.

The concept of variable pitch is illustrated in Fig. 39. The aerofoil blades in a rotor are in a fixed position as long as the incidence angle is less than that required for stall, i.e. $V_x < U \sin \alpha_s$. If the airflow incidence exceeds this angle, as would be the case with large amplitude waves, i.e., $V_x > U \sin \alpha_s$, the aerofoil is pitched in phase with the flow at angle ψ such that the incidence angle for the blades are always less than stall angle. Figure 40 shows calculations for a monoplane Wells turbine[47] for which the angle between the aerofoil chord line and the plane of rotation is increased in phase with the air flow velocities such that the airflow incidence at the hub always remains at 18°, which was assumed as the stall angle for the blades, and the maximum allowable pitch angle ψ is also 18°. It is seen from this figure that the aerodynamic efficiency of the turbine can remain high for a wide range of flow ratios and therefore the turbine has a high productivity. A similar advantage can be achieved with a pitching trailing edge flap or pitching guide vanes.

Another method by which the incidence angle to the blades can be controlled is by bypassing the airflow when the incidence exceeds the stall angle (Fig. 41). A comparison of

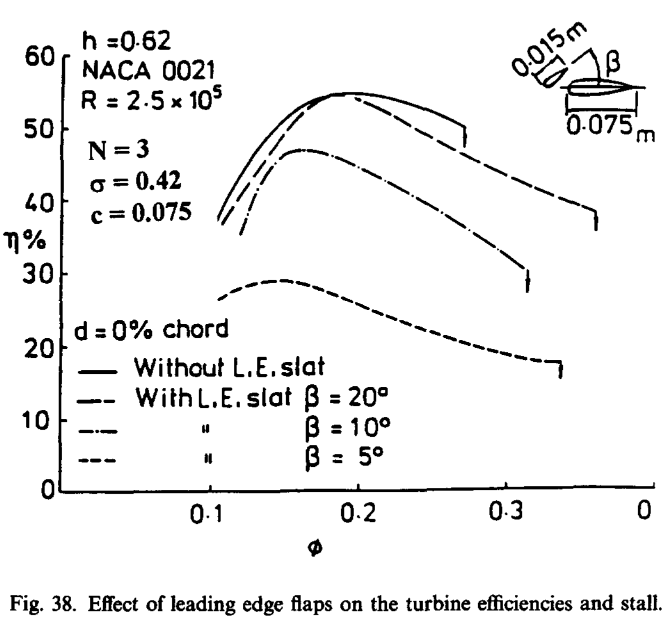

Fig. 38. Effect of leading edge flaps on the turbine efficiencies and stall.

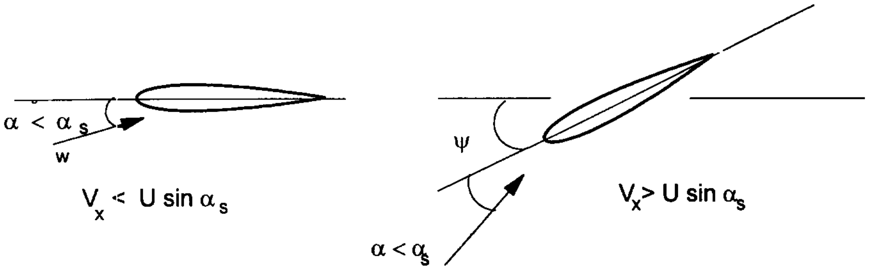

Fig. 39. A schematic diagram showing the concept of the variable pitch turbine.

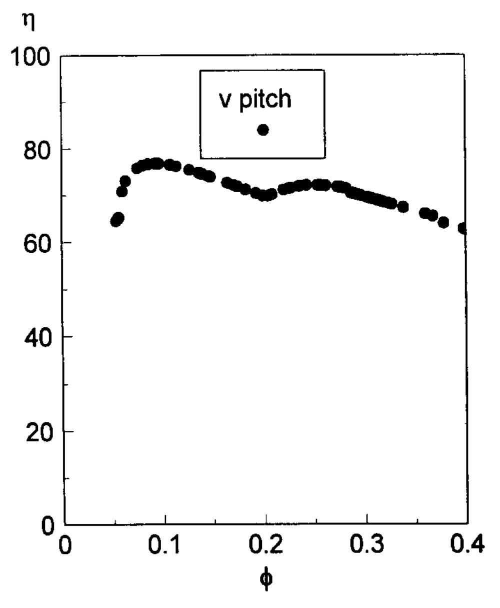

Fig. 40. The effect of variable pitch on efficiency and operational range of the Wells turbine.

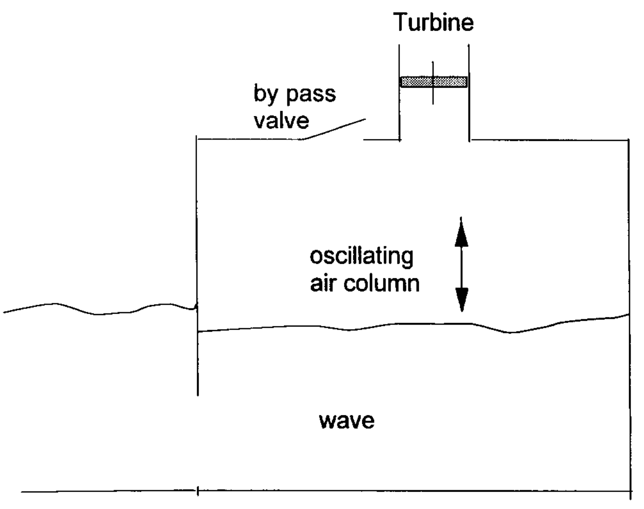

Fig. 41. A schematic diagram showing the concept of by-pass.

the by-pass concept with a variable pitch turbine,[47] for efficiencies (Fig. 42), shows that there are no appreciable differences between the two methods. It can be shown that for given sea conditions both produce approximately the same power output.

A high solidity mono plane or a biplane Wells turbine is a simple configuration but has large kinetic energy losses due to swirl at the exit. A concept which can virtually eliminate the exit losses associated with the swirl is the contra-rotating Wells turbine (Fig. 43) where the down stream rotor rotates in opposite to direction that of the upstream rotor. The directions of rotation are reversed when the flow direction is reversed.

Predictions[1, 45] for such a rotor (Fig. 44) indicates that there is considerable improvement in the overall efficiency when compared to a biplane rotor.

Passive control methods have been suggested for transonic flows but such a method is also applicable to low speed flows. Figure 45 based on computation[44] on a single aerofoil

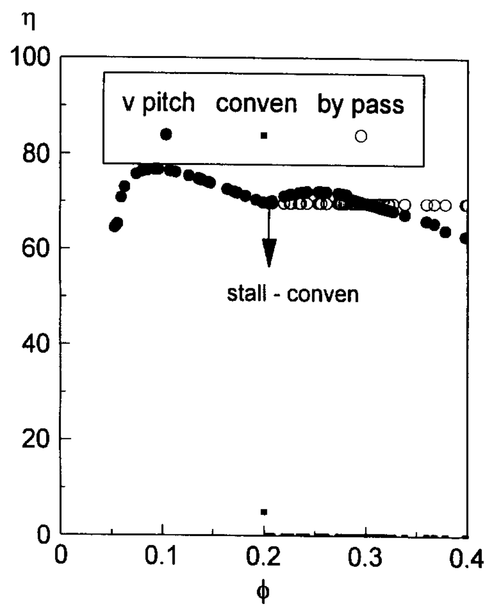

Fig. 42. A comparison of efficiencies of the Wells turbines with variable pitch or by-pass with a conventional Wells turbine.

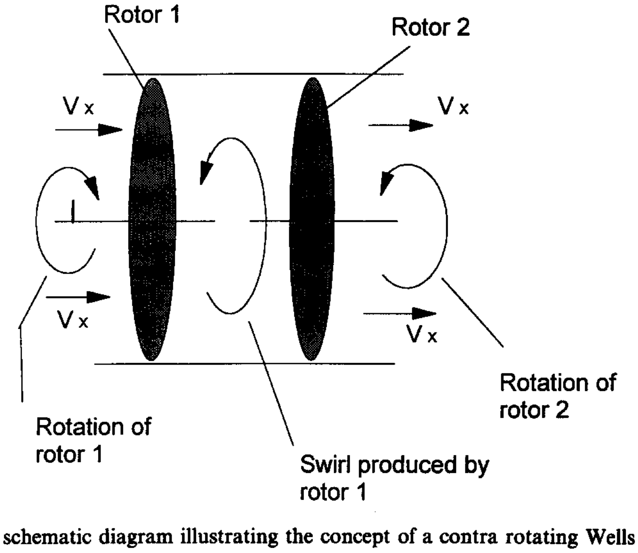

Fig. 43. A schematic diagram illustrating the concept of a contra rotating Wells turbine.

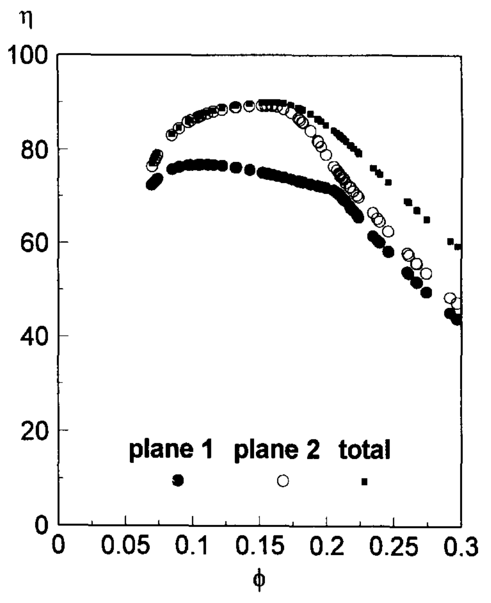

Fig. 44. The variation of efficiency with flow ratio for a contra rotating Wells turbine. D_t = 1.2 m, plane 1 at 1500 rpm, plane 2 at 1800 rpm.

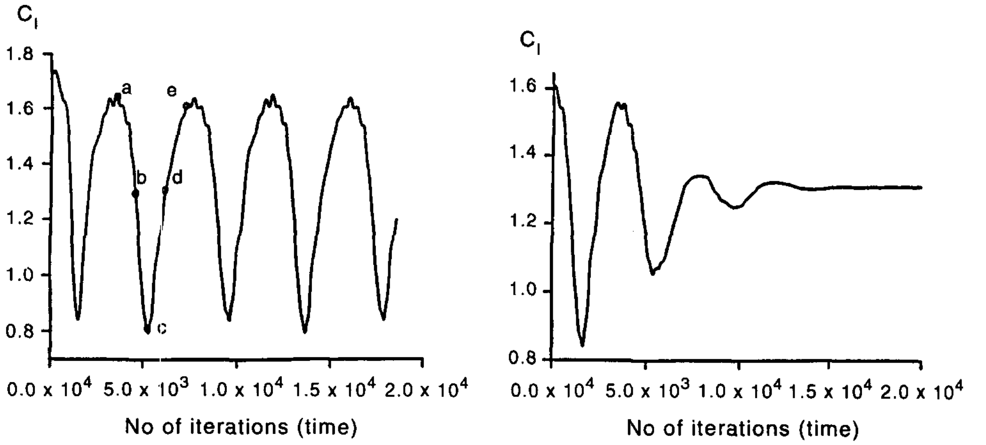

Fig. 45. Dynamic loads on an aerofoil, NACA 0012, $a = 18°$, R $= 10^6$ Transition fix at 0.03c. (a) Without passive control; (b) with passive control porosity factor 0.4 distributed between $x/c = 0.1$ and 0.9.

shows that passive boundary layer control with a porous surface and a cavity eliminates unsteady separation on an aerofoil at large incidences and produces a stable lift. This concept could be used in conjunction with the concepts based on a moving aerofoil to enhance the performance range and life span of the Wells turbine.

All these methods are, at present time, at a conceptual stage and need detailed experimental investigations on a large-scale Wells turbine with regards to both improvement in performance and cost effectiveness.

8. CONCLUDING REMARKS

Wave energy devices which are currently operational and the ones to be built in Europe and elsewhere use the concept of an oscillating water–air column for energy conversion. A key element in such energy conversion systems is the Wells turbine which rotates in a single direction in a bidirectional airflow. The aerodynamic performance of the Wells turbine is reviewed here. The Wells turbine has a linear pressure drop-flow rate characteristics which is well suited for wave energy conversion from an oscillating water column. The current prediction methods for the performance of a Wells turbine need aerodynamic data on aerofoils in a cascade of 90° stagger angle. The data available on such a cascade are based on either potential flow methods or semiempirical theory which, although only accurate to first order, agrees favourably with small-scale experiments. There are discrepancies between predictions and experiments conducted on a large-scale Wells turbine in a wave energy device at sea and this is largely due to experimental errors and scale effects which are not fully understood. The way forward for improving the predictions is to exploit CFD techniques.

Of the several parameters which affect the performance of Wells turbine the most important one appears to be the turbine blade solidity. It is possible to select a suitable solidity to match the turbine with a device for the pressure drop. A large solidity is needed for the turbine to be self starting. Self starting may not be an important factor in design and a large solidity is detrimental to the performance a solidity of less than 0.5 is recommended for design. The pressure drop on a mono plane Wells turbine is limited by the tip speed if the transonic flow effects are to be avoided. For wave energy devices which are designed for significantly large pressure amplitudes a multiplane turbine with or without guide vanes can be used. A multiplane turbine without guide vanes is less efficient than the one with guide vanes but is relatively simple to design and easy to maintain and repair. The performance of a biplane Wells turbine is dependent on the gap between the planes. A gap-to-chord ratio between the planes of 1.0 is recommended for the design biplane Wells turbine in order to achieve high efficiencies in a limited space.

The performance of a constant speed fixed blade Wells turbine can operate over a certain range of flow rates (sea states) and is limited by the onset of stall on the turbine blades. For sea states where significantly large axial velocities are produced in the chamber the turbine will experience buffeting which will reduce the life span of blades. A variable pitch turbine or a turbine with a bypass with some form of boundary layer control on the blades/hub can not only alleviate this problem but would also enable the turbine to generate power under a wide range of sea states.

REFERENCES

1. Beattie, W. C. and Raghunathan, S. (1993) A novel contra rotating Wells turbine. European Wave Energy Symposium, Edinburgh, Paper E5.
2. Csandy, G. T. (1964) *Theory of Turbomachines*, McGraw-Hill, London.
3. Gato, L. M. C. and Falcao, A. F. de O. (1984) On the theory of Wells turbine, *Trans. ASME. J. Eng. Gas Turbines Power*, **106**, pp. 628–633.
4. Gato, L. M. C., Falcao, A. F. de O. (1988) Aerodynamics of Wells turbine. *Int. J. Mech. Sci.* **30**, pp. 383–395.
5. Gato, L. M. C., Falcao, A. F. de O. (1988) Phase control of an OWC by a Wells turbine with swinging rotor blades, Euromechanics Colloq. 243. Energy from ocean waves, Bristol, U.K.
6. Gato, L. M. C. and Falcao, A. F. de O. (1990) Performance of Wells turbine with a double row of guide vanes, *JSME Int. J. Ser II*, **33**, pp. 265–271.
7. Grant, R. J., Johnson, C. G. and Sturge, G. P. (1981) Performance of Wells turbine for use in wave energy system, *Proc. Inst. Elect. Eng. Conf.* **132**, pp. 117–122.
8. Grant R. J. and Johnson, C. G. (1980) Performance tests on a two stage Wells turbine, Central Electricity Generating Board, *Report MM/Mech/TF*273.
9. Horlock, J. H. (1958) Axial flow compressors, Butterworth and Co, Oxford.
10. Inoue, M., Kaneko, K., Setoguchi, T. and Raghunathan, S. (1986a) Simulation of starting characteristics of Wells turbine, Paper 86-1122, *ASME Fluids Engineering Conference*, Atlanta, U.S.A.
11. Inoue, M., Kaneko, K. and Setoguchi, T. (1986b). Determination of optimum geometry of Wells turbine rotor for wave energy generator. Part 2, Energy sources and Tech. Conf. New Orleans, U.S.A. pp. 441–449.
12. Inoue, M., Kaneko, K., Setoguchi, T. and Raghunathan, S. (1986c) Starting and running characteristics of biplane Wells turbine, *5th International Symposium on Offshore Mechanics* and *Arctic Engineering*, Tokyo, Japan. pp. 604–609.
13. Inoue, M., Kaneko, K., Setoguchi, T. and Raghunathan, S. (1987a). The fundamental characteristics and future of Wells turbine for wave power generator." *Science of Machines*, **39**, pp. 275–280.
14. Inoue, M., Kaneko, K., Setoguchi, T. and Nakano, T. (1987b). Improvement of aerodynamic performance and optimum design of Wells turbine. Research in Natural Energy, Japan, SPEY 20, pp. 121–126.

15. Inoue, M., Kaneko, K., Setoguchi, T. and Saruwatari, T. (1988) "Studies on the Wells turbine for wave energy generator". *Int. J. JSME*, **31**, pp. 676–682.
16. Jakob, E. N. and Sherman, A. (1937) Aerofoil section characteristics affected by variation of Reynolds number." *NACA Report no.* 586.
17. Kaneko, K., Setoguchi, T. and Inoue, M. (1986). Performance of Wells turbine in oscillating air flow. *Proc. Energy – Sources Tech. Conf. Exhib.* New Orleans, U.S.A. pp. 447–452.
18. Kaneko, K., Raghunathan, S., Setoghchi, T. (1993) Performance of multiplane Wells turbine for wave energy conversion, *International Conference on Ocean Engineering*. Hoikodo, Japan.
19. Scholz, N. (1977) *Aerodynamics of Cascades*, AGARDograph 220.
20. Kinoshito, T., Masuda, R., Miyojima, S. and Kato, W. (1984) Study on the system of simulation for an OWC type wave energy absorber. *IST Symp. Wave Energy Utilisation*, Japan.
21. Lakshminarayana, B. (1970) Methods of predicting the tip clearance effects in axial flow turbo machines, *J. Basic Engineering*, ASME, pp. 497–511.
22. NASA SP 290 (1972) *Turbine Design and Application.*
23. Raju, V. S., Ravindran, M. and Koola, P. M. (1993) Experience on 153 kW wave energy pilot plant, *European Wave Energy Symposium*, Edinburgh, Paper G5.
24. Raghunathan, S., Tan, C. P., Wells, N. A. J. and McIlhagger, D. S. (1981) Efficiency, starting torque and prevention of runaway with Wells self rectifying air turbine. *Proc. Int. Symp. Wave Tidal Energy*, pp. 207–218, Cambridge.
25. Raghunathan, S. and Tan, C. P. (1982) Performance of Wells turbine at starting. *J. Energy* (*AIAA*) **6**, pp. 430–431.
26. Raghunathan, S. and Tan, C. P. (1983) The aerodynamic performance of Wells turbine. *J. Energy* (*AIAA*) **7**, 3, pp. 226–230.
27. Raghunathan, S. and Tan, C. P. (1983) The performance of bi-plane Wells turbine, *J. Energy* (*AIAA*) 7, pp. 741–742.
28. Raghunathan, S. and Ombaka, O. O. (1985a) The effect of air flow frequency on the performance of Wells turbine, *Int. J. Heat and Fluid Flow* **6**, pp. 127–132.
29. Raghunathan, S., and Tan, C. P. (1985b) The effect of blade profile on the performance of Wells turbine, *Int. J. Heat Fluid Flow* **6**, pp. 17–22.
30. Raghunathan, S., Tan, C. P., Ombaka, O. O. (1986a) The performance of Wells self rectifying air turbine, *Aeron. J. RAeS* **89**, pp. 369–379.
31. Raghunathan, S. (1986b) The aerodynamic aspects of Wells turbine, *Proc. 3rd International Symposium on Wave and Tidal and Small Scale Hydro Energy*, pp. 261–279, Brighton.
32. Raghunathan, S., Eves., A, Whittaker, T. J. J. and Long, A. E. (1987a) The bi-plane Wells turbine, *Proceedings of the OMAE Conference Houstan*, U.S.A.
33. Raghunathan, S., Setoguchi, T. and Kaneko, K. (1987b) The effect of inlet conditions on the performance of Wells turbine, ASME Fluids Engineering Conference Cincinnati, Paper 87-FE2, U.S.A.
34. Raghunathan, S., Setoguchi, T. and Kaneko, K. (1987c) Hysteresis on Wells turbine blades, Paper 87-FE3, *ASME Fluids Engineering Conference* Cincinnati, U.S.A.
35. Raghunathan, S. (1988) "Aerodynamic forces on aerofoils at high angles of attack." *AIAA National Fluid Dynamics Congress.* Paper 88-3697, Cincinnati, U.S.A.
36. Raghunathan, S., Harrison, S. R. and Hawkins, B. D. (1988) A thick aerofoil at low Reynolds numbers and large incidence, *J. Aircraft* **25**, pp. 669–671.
37. Raghunathan, S., Setoguchi, T. and Kaneko, K. (1989a) Correlation of test rig and wind tunnel tests for performance prediction of Wells turbine, *Proc. Offshore Mech. and Arctic Eng. Conf.*, The Hague, The Netherlands.
38. Raghunathan, S., Setoguchi, T. and Kaneko, K. (1989b) The effect of inlet conditions on the performance of Wells turbine *J. Energy Resources Tech. ASME.* **III**, pp. 37–42.
39. Raghunathan, S., Setoguchi, T. and Kaneko, K. (1989c) Some techniques to improve the operation range of the Wells turbine for wave power generator, *JSME Int. J. Series II* **32**, pp. 71–77.
40. Raghunathan, S., Setoguchi, T. and Kaneko, K. (1990) "Prediction of Wells turbine performance from aerofoil data." *J. Turbomach. ASME.* **112**, pp. 792–795.
41. Raghunathan, S., Setoguchi, T. and Kaneko, K. (1991) Aerodynamics of monoplane Wells turbine–A review. Proc. Offshore mechanics and Polar Engineering Conf, Edinburgh, U.K.
42. Raghunathan, S (1993). The prediction of the performance of bi-plane wells turbine. *Proceedings of the ISOPE Conference*, Singapore.
43. Raghunathan, S., Curran, R., McIlwain, S. T. and Whittaker, T. J. J. (1994) The prediction of Islay Wells turbine performance, Proceedings of the ISOPE Conference, Tokyo, Japan.
44. Raghunathan, S., Mitchell, D. and Gillan, M. A. (1994) Passive boundary layer control to alleviate dynamic loads on Wells turbine. *Proceedings of the ISOPE Conference*, Tokyo, Japan.
45. Raghunathan, S., and Wong, D. Aerofoils in a cascade of 90 deg. Stagger, in preparation.
46. Raghunathan, S. and Beattie, W. C. Aerodynamic performance of a contra rotating Wells turbine for wave energy conversion, in preparation.
47. Raghunathan, S. The relative merits of variable pitch and bypass for improving the performance of Wells turbine, in preparation.
48. Raghunathan, S. The design of a bi-plane Wells turbine, in preparation.
49. Ravindran, M. and Balabaskaran, V. (1993) Comparison of performance of constant and varying chord turbine rotors, European Wave Energy Symposium, Edinburgh, Paper E4.
50. Salter, S. H. (1993) Variable pitch Wells turbine, European wave energy symposium, Edinburgh, Paper P8.
51. Sekiya, S. and Ichikawa, A. (1984) Studies on a Wells turbine performance, *Preprint of the Turbomachinery Society of Japan*, **13**, pp. 94–99.
52. Sekiya, S., Ichikawa, A. and Hirai, T. (1983) Studies on a Wells turbine performance. *Preprint of Turbomachinery Society of Japan*, **12**, pp. 68–73.

53. Suzuki, M., Arakawa, T. and Tagori, T. (1984) Comparison of performance of Wells turbine with different blade shapes, *Preprint of Turbomachinery Society of Japan* **13**, pp. 62–67.
54. Sturges, D. P. (1981) Prediction of performance of Wells wave power turbine. *I. E. E. Conference*, Publication No. 192, pp. 117–122.
55. Tagori, R., Arakawa, C. and Suzuki, M. (1987) Estimation of prototype performance and optimum design of Wells turbine, *Research in Natural Energy* SPEY 20, pp. 127–132.
56. Weinig, F. (1935) Die stromung um die schaufeln von turbomaschinen, J. A. Barth, Leipzig.
57. Whittaker, T. J. T. et al. (1985a) The Queen's university of Belfast axisymmetric and multi-resonant wave energy converters, *Trans. ASME. J. Energy Resources Tech.* **107**, pp. 74–80.
58. Whittaker, T. J. T. and McPeake, F. A. (1985a) Design optimisation of axisymmetric tail tube buoys, *IUTAM Symposium on Hydrodynamics of Ocean Wave Energy* Conversion, Lisbon, July.
59. Whittaker, T. J. J., McIlwain, S. T. and Raghunathan, S. (1993) "Islay shore line wave power station". *Proceedings European Wave Energy Symposium*, Paper G6, Edinburgh.
60. White, P. R. S. (1981) The development and testing of a 1/10th scale self rectifying air turbine power conversion system. Lancaster Polytechnic Report.